BNL-112467-2016-JA

REGIONAL INFLUENCE OF AEROSOL EMISSIONS FROM WILDFIRES DRIVEN BY COMBUSTION EFFICIENCY: INSIGHTS FROM THE BBOP CAMPAIGN

Sonya Collier, Shan Zhou, Timothy B. Onasch, Daniel A. Jaffe, Lawrence Kleinman, Arthur J. Sedlacek III, Nicole Briggs, Jonathan Hee, Edward Fortner, John E. Shilling, Douglas Worsnop, Robert J. Yokelson, Caroline Parworth, Xinlei Ge, Jianzhong Xu, Zachary Butterfield, Duli Chand, Manvendra K. Dubey, Mikhail Pekour, Stephen Springston, Qi Zhang

Accepted for publication in
Environmental Science & Technology

July 2016

Biological, Environmental & Climate Sciences Dept.

Brookhaven National Laboratory

U.S. Department of Energy
USDOE Office of Science (SC),
Biological and Environmental Research (BER) (SC-23)

DISCLAIMER

Regional Influence of Aerosol Emissions from Wildfires Driven by Combustion Efficiency: Insights from the BBOP Campaign

Sonya Collier[1], Shan Zhou[1], Timothy B. Onasch[2], Daniel A. Jaffe[3], Lawrence Kleinman[4], Arthur J. Sedlacek III[4], Nicole Briggs[5], Jonathan Hee[3], Edward Fortner[2], John E. Shilling[6], Douglas Worsnop[2], Robert J. Yokelson[7], Caroline Parworth[1], Xinlei Ge[1], Jianzhong Xu[1], Zachary Butterfield[8], Duli Chand[6], Manvendra K. Dubey[8], Mikhail Pekour[6], Stephen Springston[4], Qi Zhang[1]*

[1]Department of Environmental Toxicology, University of California, Davis, CA 95616, USA
[2]Aerodyne Research Inc., Billerica, MA 01821, USA
[3]School of Science and Technology, University of Washington, Bothell, WA 98011, USA
[4] Environmental and Climate Sciences Department, Brookhaven National Laboratory, Upton, NY 11973, USA
[5]Gradient Corporation, Seattle WA 98101, USA
[6]Atmospheric Sciences and Global Change Division, Pacific Northwest National Laboratory, Richland, WA 99352, USA
[7]Department of Chemistry, University of Montana, Missoula, MT 59812, USA
[8]Earth and Environmental Sciences Division, Los Alamos National Laboratory, Los Alamos, NM 87545, USA

Keywords: biomass burning, aerosol chemistry, BBOA, modified combustion efficiency (MCE), emission factors

*Corresponding author: Qi Zhang, dkwzhang@ucdavis.edu, (530)752-5779, Department of Environmental Toxicology, University of California, 1 Shields Ave. Davis, CA 95616

Abstract

Wildfires are important contributors to atmospheric aerosols and a large source of emissions that impact regional air quality and global climate. In this study, the regional and nearfield influences of wildfire emissions on ambient aerosol concentration and chemical properties in the Pacific Northwest region of the United States were studied using real-time measurements from a fixed ground site located in Central Oregon at the Mt. Bachelor Observatory (~ 2700 m a.s.l.) as well as near their sources using an aircraft. The regional characteristics of biomass burning aerosols were found to depend strongly on the modified combustion efficiency (MCE), an index of the combustion processes of a fire. Organic aerosol emissions had negative correlations with MCE, whereas the oxidation state of organic aerosol increased with MCE and plume aging. The relationships between the aerosol properties and MCE were consistent between fresh emissions (~1 hour old) and emissions sampled after atmospheric transport (6 - 45 hours), suggesting that biomass burning organic aerosol concentration and chemical properties were strongly influenced by combustion processes at the source and conserved to a significant extent during regional transport. These results suggest that MCE can be a useful metric for describing aerosol properties of wildfire emissions and their impacts on regional air quality and global climate.

1. Introduction

Biomass burning (BB) is one of the largest sources of trace gases and carbonaceous aerosols on a global scale and has intense adverse effects on air quality and human health[1-4]. Emissions from wildfires and other BB sources, such as agricultural and residential wood burning, also influence Earth's climate via a combination of direct[2, 5], indirect[6, 7] and semi-direct effects[8, 9]. Wildfires, in particular, are a large and highly variable component of BB emissions[10] and typically an "uncontrollable" source of aerosols that can cause haze in pristine areas and poor air quality at downwind sites[11, 12]. Many factors, such as fuel type, burn conditions, and atmospheric aging, can influence the chemical and microphysical properties of BB aerosols. The organic component, namely biomass burning organic aerosol (BBOA), is a dominant component in BB fine aerosols[13, 14] and thus influences their hygroscopicity and optical properties, which are important parameters for assessing the impacts of BB emissions on regional air quality and global climate. However, BBOA are compositionally complex and their characteristics and impacts are poorly represented in models.

An important property of a BB event which strongly affects emission characteristics is the modified combustion efficiency (MCE) – an index of the relative amount of smoldering and flaming. The MCE is defined as the unitless molar ratio of the enhanced concentration of CO_2 over the background to the sum of the enhanced concentrations of CO and CO_2: $MCE = \Delta CO_2 / (\Delta CO + \Delta CO_2)$[15, 16]. Higher MCE (> 0.9) is associated with most of the emissions being processed by flaming combustion, whereas lower MCE (< 0.9) is associated with mostly smoldering combustion, where pyrolysis and gasification emissions escape flame processing[16, 17]. Various studies have demonstrated that emission factors for particulate matter (PM) and trace

gases in BB are strongly influenced by MCE[18-21] and that lower MCE is usually associated with increased PM emissions per unit of fuel burned[22-24].

So far, much of the information on BB emissions comes from prescribed and agricultural fires and very little is known about the characteristics of BBOA and their correlation with MCE for wildfires, especially in the mid-latitude region. In order to fill this knowledge gap, we examine plumes from wildfires in the Pacific Northwest region of the United States using data acquired in summer 2013 during the Department of Energy (DOE) sponsored Biomass Burning Observation Project (BBOP). The BBOP campaign combined aircraft and ground measurement platforms to study both gas and particle phase emissions using real-time instruments and collected one of the most extensive datasets on wildfires performed in the contiguous U.S. Here, we report the chemical characteristics of non-refractory submicrometer aerosols (NR-PM_1) measured by two high-resolution time-of-flight Aerosol Mass Spectrometers (HR-AMS) in regional and near-field wildfire plumes with a range of transport times (1 hour – 2 days) and their relationships to MCE and atmospheric aging that potentially refine representation of BB emissions in models for more accurate assessments of wildfire impacts.

2. Experimental Methods

2.1. Campaign Description and Instrument Deployment

As shown in Figure 1, various instances of strong and persistent wildfire activity in the Pacific Northwest region were reported by satellite data during the campaign period (July 25th-August 25th, 2013) and many wildfire plumes were sampled at a fixed site located at Mt. Bachelor Observatory (MBO; 43.979 ^{o}N, 121.687 ^{o}W, ~ 2700 m a.s.l.). In addition, fresher (~1 hour aging) plumes from the Whiskey Fire Complex and more aged plumes (4-10 hours)

89 transported from the Salmon River Fire Complex were sampled extensively by the Gulfstream
90 G-1 aircraft on Aug. 6th and 16th, respectively (Fig. 1).
91 A comprehensive suite of real-time instruments, including HR-AMS[25, 26] and
92 measurements of aerosol optical properties and gas-phase tracer concentrations, were deployed
93 on board the G-1 aircraft and at MBO during BBOP. The HR-AMS provides detailed chemical
94 information of the non-refractory (NR) portion of PM_1 at fast time-resolution and its high-
95 resolution mass spectra help identify various sources for observed ambient aerosol and determine
96 the average elemental ratios of organic components[26-28]. At MBO, the HR-AMS was operated in
97 the ion optical "V-mode" and sampled alternatively, every 5 minutes, downstream of a
98 thermodenuder instrument and through an ambient bypass line (see Fig. S1 and section 1.1.1 in
99 the Supplementary Information). For the purposes of this analysis, only bypass information is
100 discussed.
101 The G-1 platform measured aerosol composition using an HR-AMS equipped with an
102 intracavity laser, which is called the Soot-Particle Aerosol Mass Spectrometer (SP-AMS[29]).
103 Aerosol particles were sampled from outside of the G-1 using a forward facing two-stage
104 diffuser aerosol inlet system [30]. Inside the G-1, PM_1 were sampled into the SP-AMS through a
105 130 micron diameter critical orifice from a constant pressure inlet operating at a pressure of ~620
106 Torr [31]. The SP-AMS alternated between "laser-on" mode, for the measurement of refractory
107 black carbon and associated coatings, and "laser-off" mode, which functions identically to a
108 standard HR-AMS. In this study we focus on data acquired in "laser-off" mode, i.e., as a
109 standard HR-AMS, in 'V-mode'. However, unlike the HR-AMS at MBO, the SP-AMS on the G-
110 1 was operated in 'Fast-MS' mode with 1 second sampling time[32, 33].

Additional descriptions of measurements and instrumentation during BBOP are given in the Supplementary Information. Table S1 contains quality control and assurance information such as limit of detections, ionization efficiencies, and relative ionization efficiencies for both MBO and G-1. Influences from gas-phase CO_2 on the particulate organic CO_2^+ signal were subtracted in a time-dependent manner using gas-phase CO_2 data[34] for both platforms. All the data reported here has been converted to standard temperature and pressure (STP, 273 K, 1 atm) conditions.

2.2 Back Trajectory Analysis and Estimation of Plume Transport Times

The locations and times of active fires in the region, detectable by the MODIS instrument aboard the Aqua and Terra satellites, were downloaded from the NASA operated Fire Information Resource Management System (https://firms.modaps.eosdis.nasa.gov, near real-time collection 5 type data was used). In order to identify possible plume sources, 3-day back trajectory analysis was performed using the HYSPLIT model (Hybrid Single Particle Lagrangian Integrated Trajectory archive data, available at http://ready.arl.noaa.gov/HYSPLIT.php)[35]. HYSPLIT results were compared with MODIS fire hotspot information (Fig. S3-S17), where overlap of trajectories with hotspots both verified wildfire emission source locations and provided estimated plume transport times. In cases where multiple sources were possible candidates or where source or transport time was ambiguous, forward trajectory analysis was performed using 40km resolution meteorological data (EDAS). Average and ranges for transport time for each plume were estimated based on a combination of both forward and back trajectory results. When plumes occurred for G-1 the flight path coordinates were used as starting points for back trajectory analysis. When the G-1 location coincided very closely to a MODIS fire hotspot, it was assumed that plumes were approximately 1 hour old, in order to allow for plume

rise. Air mass relative humidity (RH) values along calculated trajectories were also derived via HYSPLIT back trajectory analysis.

3. Results and Discussion

3.1. Identification of wildfire plumes and calculation of MCE and enhancement ratios

Near combustion sources, emission factors and emission ratios are commonly calculated for use in emissions inventories[4]. However, MCE and enhancement ratios (ERs) can be calculated for emissions sampled downwind of a fire source by taking the ratio of the enhancement of a species of interest above background to the enhancement of a stable representative plume tracer. ERs may also be calculated by finding the linear regression slope between a parameter of interest and the plume tracer when multiple, well-correlated measurements are available at a specific distance downwind[36, 37]. Changing backgrounds, particularly when plumes enter a different air mass such as the free troposphere, can impact calculation of MCE and ERs for trace gases and particulate species in BB plumes[38]. However, uncertainty for ER calculations is much reduced when emissions of parameters of interest are significantly higher than their background values[37, 38].

In this study, we identify wildfire plumes and determine MCEs and ERs for selected periods when concentrations of CO, CO_2, organic PM, and major organic ions in the HR-AMS spectra are all well above their corresponding background levels and the correlations among these parameters are high for selected plumes[39]. The high correlation criterion is chosen to minimize background and mixing effects on MCE and ER calculations. In this study, a total of 32 plumes, 18 from MBO and 14 from G-1, are identified and the correlations between CO and CO_2 and between organic PM and ΣC (= $CO+CO_2$) are high for each plume ($r^2 > 0.85$; Fig. 2 and Table S2). Due to the stringent criteria, plumes in this analysis make up a small percentage of all

157 campaign data (e.g., 1.3% of MBO data). The correlations between HR-AMS organic ions and
158 ΣC are high for all the plumes as well (e.g., Fig. S19-S20). Note that measurements taken from
159 the G-1 are elevated relative to MBO due to their proximity to fire sources (Fig. 2).
160 For each identified plume, MCE is calculated by determining the slope between CO and
161 CO_2 using an unconstrained linear orthogonal distance regression and subsequently solving for
162 $MCE = 1/(1+\Delta CO/\Delta CO_2)$. The ERs of various aerosol and gas-phase parameters with respect to
163 ΣC for each plume are also calculated and expressed as $\Delta X/\Delta \Sigma C$, where X is a plume parameter
164 of interest. The calculated MCE values range from 0.80 to 0.99 for the 18 plumes sampled at
165 MBO and range from 0.86 to 0.96 for the 14 plumes sampled by the G-1. The ERs for most
166 aerosol parameters with respect to ΣC were found to have a strong negative correlation with
167 MCE and will be discussed further in sections 3.2 and 3.3. Most of the plumes appeared to come
168 from fires occurring in southwest Oregon and northern California with a few arriving from
169 northern Oregon (Fig. S3-S17). Based on HYSPLIT air mass trajectories and MODIS fire
170 locations, we estimate that the 32 BB plumes varied in their transport times between 1 - 48
171 hours.
172 *3.2. A case study of 3 consecutive plumes observed at MBO*
173 Fig. 3 shows an example of the identification of three BB plumes that impacted MBO on
174 August 14^{th} and 15^{th} consecutively. These plumes all came from the Salmon River Fire Complex
175 with a total transport time of approximately 12 hours, suggesting that they had undergone a
176 similar degree of atmospheric aging. Meteorological conditions were relatively stable during the
177 designated plume time spans and wind was relatively constant (12 ± 2.9 m/s, southwesterly, Fig.
178 3a). CO and CO_2 mixing ratios, aerosol scattering coefficient, and organic PM_1 mass
179 concentrations were elevated during each plume period and had high inter-correlation (Fig. 3).

The MCE values of the three plumes decreased over time at 0.91, 0.88, and 0.86 (Fig. 3b), indicating gradually decreased combustion efficiency.

BBOA is a dominant aerosol component in these plumes, accounting for > 94% of the NR-PM_1 mass. The enhancement of BBOA relative to ΣC (i.e., ΔOrg/ΔΣC) increases as MCE decreases (Fig. 3c), so do the enhancements of scattering (550nm, Fig. 3d) and the AMS marker ions for anhydrous sugars (e.g., levoglucosan) – $C_2H_4O_2^+$ (Fig. 3e) and $C_3H_5O_2^+$ [40, 41]. Inorganic nitrate (NO_3^-, Fig. 3f), although contributing a small percentage to the PM_1 mass, displays an enhancement that also correlates inversely with MCE. On the other hand, sulfate correlates less well with ΣC and does not appear significantly enhanced within the plume relative to non-plume periods (Fig. 3g), indicating influences from sources other than wildfires. Since transport time and source are similar for all three plumes, the differences observed in ERs for BBOA, tracers, scattering and inorganic nitrate are likely due to changes in combustion processes.

3.3 Influence of MCE on aerosol emission characteristics

The trends observed for the three consecutive plumes discussed above were also observed when examining all 32 plumes (Fig. 4). A strong negative correlation between the ER of BBOA and MCE is observed and the values measured from both MBO and G-1 fall tightly along the same trend (Fig. 4a). Since the estimated ages of the 32 BB plumes vary between ~1 – 48 hours (6 – 48 hours for MBO plumes and 1 – 6 hours for G-1 plumes), this strong agreement suggests that net changes in BBOA concentrations were either slow or very similar plume to plume (i.e., independent to transport time).

One explanation is that BBOA is composed of primary organic aerosol (POA) directly emitted from the burning biomass and secondary organic aerosol (SOA) formed via oxidative processing of organic gases. These two components are expected to exhibit opposite behaviors

during transport, with POA evaporating with dilution due to the semi-volatile nature of BBOA[42] and SOA increasing with more atmospheric processing[43]. Indeed, thermal denuder data from MBO demonstrates the semi-volatile nature of regional BBOA. Substantial net formation of SOA in BB emissions has been observed both in the laboratory[44-46] and in the field[47], though other field studies have not found significant enhancement of BBOA mass as BB emissions photochemically aged[36, 48, 49]. This observed variability highlights the importance of fully characterizing BBOA properties and the complex processing that modifies these properties during atmospheric transport.

Our observations of negligible change in the apparent ERs of BBOA with transport time for a range of MCE values might be a combined, offsetting outcome of primary BBOA losses driven by dilution and subsequent evaporation of the semi-volatile components[42], and SOA formation. On the other hand, the consistency among plumes measured in this work from the G-1 and MBO may reflect some similar processing among plumes or fast processing (e.g., < 1 hour), which occurred near the source prior to sampling, then followed by little net change in BBOA during subsequent atmospheric transport.

Additionally, Fig. 4b shows the enhancement with respect to ΔCO, which is often used to determine net formation of secondary components due to photochemical activity, particularly for transported plumes since CO is a stable tracer and has negligible background concentrations. However, it is important to note that the relative amount of CO emitted is influenced by MCE as well. CO increases with decreasing MCE, thus ΔOrg/ΔCO is relatively flat for various MCEs and there is high consistency between MBO and G-1 plumes (Fig. 4b) with the exception of plume 14 at MCE = 0.8 which has a significantly larger enhancement. Based on back-trajectory analysis, this plume appears to be of similar age to other plumes but originated from the Douglas

Complex Fire, which was less frequently sampled at MBO during this study. Thus the larger ΔOrg/ΔCO for this plume could be characteristic of smoldering fires, which are associated with higher VOC emissions and lower NOx[17, 18], conditions which may lead to higher SOA forming potential over a wide range of aging time. Or larger ΔOrg/ΔCO could be due to differences in fuel type. Caution should be taken in this interpretation since a limited number of plumes were sampled in the lower MCE range (0.8-0.85).

A strong negative correlation of the ERs of the HR-AMS levoglucosan tracer ion ($C_2H_4O_2^+$ [41, 50]) and MCE is observed (Fig. 4c), indicating that anhydrous sugars are emitted in larger quantities under less efficient combustion. This is consistent with the increased emissions of incomplete combustion products under more smoldering conditions. Furthermore, the overlap in ERs of this tracer ion in fresher and more aged plumes (Fig. 4b-4c) suggests few or similar losses of anhydrous sugars during atmospheric transport. Previous studies indicate that levoglucosan can undergo oxidation in the atmosphere[45], particularly under cloudy conditions[51]. We therefore examine relative humidity (RH) along each MBO plume trajectory derived via HYSPLIT back trajectory analysis and summarize the results of this analysis in Fig. S18. According to RH values of air masses, all plumes experienced dry conditions (mean RH = 39% ± 9.6%) along their trajectories before sampling at MBO, suggesting that aqueous oxidation was less likely to have affected levoglucosan enhancement ratios during this study.

The ER of aerosol light scattering determined from MBO clearly decreases as a function of MCE (Fig. 4d), similar to the trend observed for the ER of organic aerosols (Fig. 4a). However, those from G-1 measurements appear to deviate from the trend (Fig. 4d), likely due to different size cutoff for particle sampling: MBO used a PM_1 inlet while G-1 used an isokinetic

248 inlet (samples particles up to 5 μm in size), thus additionally may have measured the scattering
249 of coarse mode soil and dust particles.

250 The ERs of nitrate measured at MBO correlate inversely with MCE whereas those
251 measured from G-1 have a more flat behavior (Fig. 4e). Typically ERs of nitrogen-containing
252 compounds measured near the source are indicative of fuel nitrogen content[15]. Oxidized
253 compounds such as NO_x dominate in flaming conditions whereas reduced compounds such as
254 NH_3 dominate in smoldering conditions[16]. In this case, however, the transport of these plumes
255 complicates the interpretation. Due to photochemical processes, NO_x can be converted to more
256 oxidized components such as peroxyacetyl nitrate (PAN) and nitrate[52]. On the other hand, sulfate
257 often displays poor correlations with ΣC and its ER values show little dependence on MCE (Fig.
258 4f). These observations are consistent with previous findings that S content in biomass is highly
259 variable and that the EF of S-containing species displays weak correlation with MCE in
260 laboratory fires[19, 53]. The contributions of wildfires to sulfate appeared negligible compared to
261 background concentrations during this study and hence, sulfate appeared to be contributed by
262 sources other than wildfires.

263 *3.4 Influence of MCE on Chemical Properties of Organic Aerosol in Biomass Burning*
264 *Plumes*

265 The chemical properties of BBOA observed for individual plumes are examined to
266 determine whether a relationship between the organic aerosol chemistry and MCE existed or
267 whether atmospheric aging had a larger influence. In this study, and ambient air in general, BB
268 plumes often occurred as short-duration events over an elevated background of more aged
269 aerosols. In order to isolate signals unique to the targeted plume from background contributions,
270 we determined the ERs of the organic-equivalent mass concentrations of ions measured by the

AMS by calculating their unconstrained linear regression slope with respect to ΣC. We defined an enhancement ratio mass spectrum (ERMS) by using the calculated slope of each ion as the signal contribution in the new ERMS and then normalized the total signal in the ERMS to 1. All 32 BB plumes were treated in the same way and a unique ERMS was derived for each plume to examine detailed chemical information of BBOA, such as elemental ratios (e.g., O/C and H/C), carbon oxidation state (OS_C), and fractional contributions of tracer ions (e.g., $f_{C2H4O2+}$). Note that for each plume, a vast majority of the ions show tight correlations with ΣC ($r^2 > 0.9$; e.g., see Supplementary Fig. S19-S20), which indicates the validity of using this approach to extract plume spectra. Ions with lower r^2 were retained, but they contribute < 5% of the overall signal in the ERMS and consequently, their influence on calculated elemental ratios is considered negligible.

Fig. 5 shows the chemical properties of BBOA derived from the ERMS of the 32 plumes as a function of MCE. The $f_{C2H4O2+}$ is used to assess the influence of BB on ambient aerosol [40]. Findings from lab studies regarding $f_{C2H4O2+}$ and combustion conditions have been variable with a residential wood burning experiment showing a positive correlation of $f_{C2H4O2+}$ with MCE[54] and a simulated open burning experiment finding similar $f_{C2H4O2+}$ for both smoldering and flaming[41]. In this study a decreasing trend with respect to MCE is observed for both the fresh (~1-6 hours of transport) and more aged (6-48 hours of transport) plumes with very good agreement between the observations from MBO and G-1 (Fig. 5a). These results reinforce the conclusion that the ERs of levoglucosan measured downwind appear to reflect those measured near the source, and that subsequent processing was either minimal or similar in all plumes. While a decrease of $f_{C2H4O2+}$ has been shown to correlate with aging of BBOA[40, 55], our analysis suggests that MCE is an additional factor affecting $f_{C2H4O2+}$ for BBOA with less than 48 hours of atmospheric aging.

294 Hence caution should be exercised while using this tracer to probe the evolution of biomass
295 burning aerosols in the atmosphere.
296 The H/C has a decreasing trend with respect to MCE (Fig. 5b) whereas O/C increases
297 with MCE (Fig. 5c). In addition, OS_C (= 2×O/C – H/C), which is a more reliable metric for
298 describing the average carbon oxidation state of organic aerosol[56], also shows an increasing trend
299 with MCE (Fig. 5d). Other studies have measured the fractional contribution of CO_2^+, a
300 dominant ion fragment in highly oxidized organic aerosol[57], to total BBOA signal (f_{44}) for
301 various fuels under controlled conditions[54, 58-60]. One lab study showed that f_{44} could vary in its
302 dependence on MCE by fuel type, suggesting some fuel types led to more oxidized organic
303 aerosol in flaming conditions[60]. Our results indicate relatively greater emissions of reduced
304 organic compounds at lower MCE values, which is consistent with smoldering combustion (low
305 MCE) emitting higher concentrations of both particulate and gaseous organic compounds and
306 with BBOA often appearing semi-volatile in nature. As MCE increases, the overall composition
307 of BBOA becomes more oxidized and possibly less volatile. Furthermore, since the ER of
308 BBOA is lower at high MCE, differential evaporation may cause preferential partitioning to the
309 gas-phase of the semi-volatile species, leaving a higher fraction of more oxidized components[61].
310 However, the trends for O/C and OS_C as a function of MCE are not as clear for the fresher
311 plumes sampled by G-1 closer to the fire sources and the G-1 plumes tend to be less oxidized
312 overall compared to the more aged plumes sampled at MBO.
313 In order to investigate the effect that aging may have on the observed trends, all
314 parameters in Fig. 5a-d are colored by transport times estimated based on HYSPLIT trajectories
315 and approximate overlap with MODIS fire hotspots and the relationship between O/C and OS_C
316 and transport is shown explicitly in Fig. 5e-d. Although relatively high uncertainty likely exists

317 in the estimated transport time, the results suggest that transport time plays a larger role than
318 MCE in determining the oxidation state of transported BBOA. In general, older plumes appear
319 more oxidized for a given MCE value and the correlation between oxidation state and plume age
320 appears somewhat higher (Fig. 5e-f) than that between BBOA oxidation and MCE (Fig. 5c-d).
321 Nevertheless, MCE appears to be another factor affecting the average oxidation state of BBOA
322 since a positive correlation is still visible. For instance, plumes at the highest MCE, despite
323 having a large range in transport times, have significantly higher OS_C compared to lower MCE
324 plumes (Fig. 5d).

325 Smoldering combustion is dominated by the gasification of unburned fuel whereas
326 flaming combustion is dominated by pyrolysis products which undergo in-flame processing[16].
327 The results shown here demonstrate that the two burning regimes, along with atmospheric aging,
328 may have affected the aerosol compositions measured downwind of the source, which tend to
329 control particle properties and hence strongly influence their impact on regional air quality and
330 climate change. This finding has important implications on our understanding of BBOA
331 properties and how we model it to further understand the effects of BB emissions on a regional
332 scale.

333 *3.5 Implications for models and emissions inventories*

334 Our study has measured ERs and MCE values for a large number of wildfire plumes and
335 highlights the dependence of aerosol emissions on MCE. Table 1 summarizes the average ERs
336 for all 32 plumes as well as for smoldering- and flaming-dominated conditions separately. Since
337 the fuel complexes discussed in this study are representative of the Pacific Northwest, our results
338 are highly relevant for understanding typical temperate wildfires of evergreen vegetation.
339 Emission ratios for similar biomes are shown for comparison in Fig. 6, where a variety of

sampling methods were used (See Table S3 for calculation method). The ERs of total organic carbon (OC) for our flaming plumes identified in this study (average ± 1σ = 0.017 ± 0.010 gC/gC; Table 1) compare well with literature "fire-average" results[4, 19, 62]; however, the ERs of OC for the smoldering plumes (0.049 ± 0.028) are significantly higher than those reported by Alves, et al.[62] and Akagi, et al.[4] although our results fall within some lab-derived OC ER reported in McMeeking, et al.[19] save two plumes with MCE < 0.85. This illustrates that the emissions from a fire temporarily dominated by smoldering may not be well represented by fire-average emissions reported in literature.

Previous studies have demonstrated that MCE is a relevant parameter controlling emission factors for BB emissions near their source[18-21, 63]. Here we have found evidence that downwind ERs describing regional BBOA concentrations as well as chemical composition are influenced by MCE at the time of emission, implying that some of the relationships controlled by combustion processes at the source survived regional transport (< 48 hours). We have also demonstrated that the oxidation state of transported BBOA appears to be affected by both atmospheric aging and MCE. These results may serve in the future for modeling PM and trace gas emissions for this region. Furthermore, the method used in this study to identify plumes and extract enhancement ratio mass spectra as a function of MCE could be applied to data from other regions to explore broader applications and further understand the relationship between fuel types, combustion processes, and atmospheric aging on observed BBOA chemistry.

Acknowledgements

This work was funded by US Department of Energy (DOE) Atmospheric Radiation Measurement (ARM) program and the Atmospheric System Research (ASR) program (Grants DE-SC0014620, DE-SC0007178, and DE-SC0014287) and used data from the ARM Climate

Research Facility, a DOE Office of Science User Facility. MBO receives funding from the National Science Foundation (Grant NSF-1447832 to DJ). R.Y. was supported by NASA ACCDAM award NNX14AP45G. The Pacific Northwest National Laboratory is operated for DOE by Battelle Memorial Institute under contract DE-AC05-76RL01830. We acknowledge the use of MODIS fire hotspot data and imagery from LANCE FIRMS, downloadable from https://firms.modaps.eosdis.nasa.gov and operated by the NASA/GSFC/Earth Science Data and Information System (ESDIS) with funding provided by NASA/HQ.

Supporting Information

Supporting information contains detailed instrumental description and campaign overview with accompanying figures, back trajectory and forward trajectory analysis results, and tables summarizing main parameters described in main manuscript.

References

1. de Gouw, J.; Jimenez, J. L., Organic Aerosols in the Earth's Atmosphere. *Environmental Science & Technology* **2009,** *43*, (20), 7614-7618.
2. Bond, T. C.; Doherty, S. J.; Fahey, D. W.; Forster, P. M.; Berntsen, T.; DeAngelo, B. J.; Flanner, M. G.; Ghan, S.; Kärcher, B.; Koch, D.; Kinne, S.; Kondo, Y.; Quinn, P. K.; Sarofim, M. C.; Schultz, M. G.; Schulz, M.; Venkataraman, C.; Zhang, H.; Zhang, S.; Bellouin, N.; Guttikunda, S. K.; Hopke, P. K.; Jacobson, M. Z.; Kaiser, J. W.; Klimont, Z.; Lohmann, U.; Schwarz, J. P.; Shindell, D.; Storelvmo, T.; Warren, S. G.; Zender, C. S., Bounding the role of black carbon in the climate system: A scientific assessment. *Journal of Geophysical Research: Atmospheres* **2013,** *118*, (11), 5380-5552.
3. Jaffe, D. A.; Wigder, N. L., Ozone production from wildfires: A critical review. *Atmospheric Environment* **2012,** *51*, (0), 1-10.
4. Akagi, S. K.; Yokelson, R. J.; Wiedinmyer, C.; Alvarado, M. J.; Reid, J. S.; Karl, T.; Crounse, J. D.; Wennberg, P. O., Emission factors for open and domestic biomass burning for use in atmospheric models. *Atmos. Chem. Phys.* **2011,** *11*, (9), 4039-4072.
5. Hobbs, P. V.; Reid, J. S.; Kotchenruther, R. A.; Ferek, R. J.; Weiss, R., Direct Radiative Forcing by Smoke from Biomass Burning. *Science* **1997,** *275*, (5307), 1777-1778.
6. Andreae, M. O.; Rosenfeld, D., Aerosol–cloud–precipitation interactions. Part 1. The nature and sources of cloud-active aerosols. *Earth-Science Reviews* **2008,** *89*, (1–2), 13-41.
7. Carrico, C. M.; Petters, M. D.; Kreidenweis, S. M.; Sullivan, A. P.; McMeeking, G. R.; Levin, E. J. T.; Engling, G.; Malm, W. C.; Collett, J. L., Water uptake and chemical composition of fresh aerosols generated in open burning of biomass. *Atmospheric Chemistry and Physics* **2010,** *10*, (11), 5165-5178.

8. IPCC, IPCC - Climate Change 2013: The Physical Science Basis. **2013**.
9. Andreae, M. O.; Rosenfeld, D.; Artaxo, P.; Costa, A. A.; Frank, G. P.; Longo, K. M.; Silva-Dias, M. A. F., Smoking Rain Clouds over the Amazon. *Science* **2004,** *303*, (5662), 1337-1342.
10. Duncan, B. N.; Martin, R. V.; Staudt, A. C.; Yevich, R.; Logan, J. A., Interannual and seasonal variability of biomass burning emissions constrained by satellite observations. *Journal of Geophysical Research-Atmospheres* **2003,** *108*, (D2), ACH 1-1 - ACH 1-22.
11. Brewer, P.; Moore, T., Source Contributions to Visibility Impairment in the Southeastern and Western United States. *Journal of the Air & Waste Management Association* **2009,** *59*, (9), 1070-1081.
12. Jaffe, D.; Hafner, W.; Chand, D.; Westerling, A.; Spracklen, D., Interannual Variations in PM2.5 due to Wildfires in the Western United States. *Environmental Science & Technology* **2008,** *42*, (8), 2812-2818.
13. Peltier, R. E.; Sullivan, A. P.; Weber, R. J.; Brock, C. A.; Wollny, A. G.; Holloway, J. S.; de Gouw, J. A.; Warneke, C., Fine aerosol bulk composition measured on WP-3D research aircraft in vicinity of the Northeastern United States: results from NEAQS. *Atmos. Chem. Phys.* **2007,** *7*, (12), 3231-3247.
14. Vicente, A.; Alves, C.; Calvo, A. I.; Fernandes, A. P.; Nunes, T.; Monteiro, C.; Almeida, S. M.; Pio, C., Emission factors and detailed chemical composition of smoke particles from the 2010 wildfire season. *Atmospheric Environment* **2013,** *71*, (0), 295-303.
15. Lobert, J. M.; Scharffe, D. H.; Hao, W. M.; Kuhlbusch, T. A.; Seuwan, R.; Warneck, P.; Crutzen, P. J., Experimental evaluation of biomass burning emissions: nitrogen and carbon containing compounds. In *Global Biomass Burning: Atmospheric, Climatic and Biospheric Implications*, Levine, J. S., Ed. MIT Press: Cambridge, MA, 1991; pp 289-304.
16. Yokelson, R. J.; Griffith, D. W. T.; Ward, D. E., Open-path Fourier transform infrared studies of large-scale laboratory biomass fires. *Journal of Geophysical Research: Atmospheres* **1996,** *101*, (D15), 21067-21080.
17. Yokelson, R. J.; Susott, R.; Ward, D. E.; Reardon, J.; Griffith, D. W. T., Emissions from smoldering combustion of biomass measured by open-path Fourier transform infrared spectroscopy. *Journal of Geophysical Research: Atmospheres* **1997,** *102*, (D15), 18865-18877.
18. Akagi, S. K.; Yokelson, R. J.; Burling, I. R.; Meinardi, S.; Simpson, I.; Blake, D. R.; McMeeking, G. R.; Sullivan, A.; Lee, T.; Kreidenweis, S.; Urbanski, S.; Reardon, J.; Griffith, D. W. T.; Johnson, T. J.; Weise, D. R., Measurements of reactive trace gases and variable O3 formation rates in some South Carolina biomass burning plumes. *Atmos. Chem. Phys.* **2013,** *13*, (3), 1141-1165.
19. McMeeking, G. R.; Kreidenweis, S. M.; Baker, S.; Carrico, C. M.; Chow, J. C.; Collett, J. L.; Hao, W. M.; Holden, A. S.; Kirchstetter, T. W.; Malm, W. C.; Moosmüller, H.; Sullivan, A. P.; Wold, C. E., Emissions of trace gases and aerosols during the open combustion of biomass in the laboratory. *Journal of Geophysical Research: Atmospheres* **2009,** *114*, (D19), D19210.
20. Yokelson, R. J.; Burling, I. R.; Urbanski, S. P.; Atlas, E. L.; Adachi, K.; Buseck, P. R.; Wiedinmyer, C.; Akagi, S. K.; Toohey, D. W.; Wold, C. E., Trace gas and particle emissions from open biomass burning in Mexico. *Atmospheric Chemistry and Physics* **2011,** *11*, (14), 6787-6808.
21. Burling, I. R.; Yokelson, R. J.; Akagi, S. K.; Urbanski, S. P.; Wold, C. E.; Griffith, D. W. T.; Johnson, T. J.; Reardon, J.; Weise, D. R., Airborne and ground-based measurements of the trace gases and particles emitted by prescribed fires in the United States. *Atmos. Chem. Phys.* **2011,** *11*, (23), 12197-12216.

22. Liu, S.; Aiken, A. C.; Arata, C.; Dubey, M. K.; Stockwell, C. E.; Yokelson, R. J.; Stone, E. A.; Jayarathne, T.; Robinson, A. L.; DeMott, P. J.; Kreidenweis, S. M., Aerosol single scattering albedo dependence on biomass combustion efficiency: Laboratory and field studies. *Geophysical Research Letters* **2014,** *41*, (2), 2013GL058392.
23. Janhäll, S.; Andreae, M. O.; Pöschl, U., Biomass burning aerosol emissions from vegetation fires: particle number and mass emission factors and size distributions. *Atmos. Chem. Phys.* **2010,** *10*, (3), 1427-1439.
24. McMeeking, G. R.; Fortner, E.; Onasch, T. B.; Taylor, J. W.; Flynn, M.; Coe, H.; Kreidenweis, S. M., Impacts of nonrefractory material on light absorption by aerosols emitted from biomass burning. *Journal of Geophysical Research: Atmospheres* **2014,** *119*, (21), 12,272-12,286.
25. Canagaratna, M.; Jayne, J.; Jimenez, J. L.; Allan, J. A.; Alfarra, R.; Zhang, Q.; Onasch, T.; Drewnick, F.; Coe, H.; Middlebrook, A.; Delia, A.; Williams, L.; Trimborn, A.; Northway, M.; DeCarlo, P.; Kolb, C.; Davidovits, P.; Worsnop, D., Chemical and Microphysical Characterization of Ambient Aerosols with the Aerodyne Aerosol Mass Spectrometer. *Mass Spectrometry Reviews* **2007,** *26*, 185-222, DOI:10.1002/mas.20115.
26. DeCarlo, P. F.; Kimmel, J. R.; Trimborn, A.; Northway, M. J.; Jayne, J. T.; Aiken, A. C.; Gonin, M.; Fuhrer, K.; Horvath, T.; Docherty, K. S.; Worsnop, D. R.; Jimenez, J. L., Field-Deployable, High-Resolution, Time-of-Flight Aerosol Mass Spectrometer. *Analytical Chemistry* **2006,** *78*, (24), 8281-8289.
27. Aiken, A. C.; DeCarlo, P. F.; Kroll, J. H.; Worsnop, D. R.; Huffman, J. A.; Docherty, K.; Ulbrich, I. M.; Mohr, C.; Kimmel, J. R.; Sueper, D.; Sun, Y.; Zhang, Q.; Trimborn, A.; Northway, M.; Ziemann, P. J.; Canagaratna, M. R.; Onasch, T. B.; Alfarra, M. R.; Prevot, A. S. H.; Dommen, J.; Duplissy, J.; Metzger, A.; Baltensperger, U.; Jimenez, J. L., O/C and OM/OC Ratios of Primary, Secondary, and Ambient Organic Aerosols with a High Resolution Time-of-Flight Aerosol Mass Spectrometer. *Environ. Sci. and Technol.* **2008,** *42*, (12), 4478-4485.
28. Canagaratna, M. R.; Jimenez, J. L.; Kroll, J. H.; Chen, Q.; Kessler, S. H.; Massoli, P.; Hildebrandt Ruiz, L.; Fortner, E.; Williams, L. R.; Wilson, K. R.; Surratt, J. D.; Donahue, N. M.; Jayne, J. T.; Worsnop, D. R., Elemental ratio measurements of organic compounds using aerosol mass spectrometry: characterization, improved calibration, and implications. *Atmos. Chem. Phys.* **2015,** *15*, (1), 253-272.
29. Onasch, T. B.; Trimborn, A.; Fortner, E. C.; Jayne, J. T.; Kok, G. L.; Williams, L. R.; Davidovits, P.; Worsnop, D. R., Soot Particle Aerosol Mass Spectrometer: Development, Validation, and Initial Application. *Aerosol Science and Technology* **2012,** *46*, (7), 804-817.
30. Brechtel, F. *Description and assessment of a new aerosol inlet for the DOE G-1 research aircraft, Final technical report of work performed by BMI under contract #0000058843*; Brookhaven National Laboratory: 2003.
31. Bahreini, R.; Dunlea, E. J.; Matthew, B. M.; Simons, C.; Docherty, K. S.; DeCarlo, P. F.; Jimenez, J. L.; Brock, C. A.; Middlebrook, A. M., Design and Operation of a Pressure-Controlled Inlet for Airborne Sampling with an Aerodynamic Aerosol Lens. *Aerosol Science and Technology* **2008,** *42*, (6), 465-471.
32. Lack, D. A.; Corbett, J. J.; Onasch, T.; Lerner, B.; Massoli, P.; Quinn, P. K.; Bates, T. S.; Covert, D. S.; Coffman, D.; Sierau, B.; Herndon, S.; Allan, J.; Baynard, T.; Lovejoy, E.; Ravishankara, A. R.; Williams, E., Particulate emissions from commercial shipping: Chemical, physical, and optical properties. *Journal of Geophysical Research: Atmospheres* **2009,** *114*, (D7), D00F04.

33. Kimmel, J. R.; Farmer, D. K.; Cubison, M. J.; Sueper, D.; Tanner, C.; Nemitz, E.; Worsnop, D. R.; Gonin, M.; Jimenez, J. L., Real-time aerosol mass spectrometry with millisecond resolution. *International Journal of Mass Spectrometry* **2011,** *303*, (1), 15-26.
34. Collier, S.; Zhang, Q., Gas-Phase CO2 Subtraction for Improved Measurements of the Organic Aerosol Mass Concentration and Oxidation Degree by an Aerosol Mass Spectrometer. *Environmental Science & Technology* **2013,** *47*, (24), 14324-14331.
35. Draxler, R. R.; Hess, G., An overview of the HYSPLIT_4 modelling system for trajectories. *Australian meteorological magazine* **1998,** *47*, (4), 295-308.
36. Jolleys, M. D.; Coe, H.; McFiggans, G.; Capes, G.; Allan, J. D.; Crosier, J.; Williams, P. I.; Allen, G.; Bower, K. N.; Jimenez, J. L.; Russell, L. M.; Grutter, M.; Baumgardner, D., Characterizing the Aging of Biomass Burning Organic Aerosol by Use of Mixing Ratios: A Meta-analysis of Four Regions. *Environmental Science & Technology* **2012,** *46*, (24), 13093-13102.
37. Briggs, N. L.; Jaffe, D. A.; Gao, H.; Hee, J.; Baylon, P.; Zhang, Q.; Zhou, S.; Collier, S.; Sampson, P.; Cary, R. A., Particulate matter, ozone, and nitrogen species in aged wildfire plumes observed at the Mount Bachelor Observatory, a high elevation site in the Pacific Northwest. *Aerosol and Air Quality Research* **2016,** *Accepted*.
38. Yokelson, R. J.; Andreae, M. O.; Akagi, S. K., Pitfalls with the use of enhancement ratios or normalized excess mixing ratios measured in plumes to characterize pollution sources and aging. *Atmos. Meas. Tech.* **2013,** *6*, (8), 2155-2158.
39. Wigder, N. L.; Jaffe, D. A.; Saketa, F. A., Ozone and particulate matter enhancements from regional wildfires observed at Mount Bachelor during 2004–2011. *Atmospheric Environment* **2013,** *75*, (0), 24-31.
40. Cubison, M. J.; Ortega, A. M.; Hayes, P. L.; Farmer, D. K.; Day, D.; Lechner, M. J.; Brune, W. H.; Apel, E.; Diskin, G. S.; Fisher, J. A.; Fuelberg, H. E.; Hecobian, A.; Knapp, D. J.; Mikoviny, T.; Riemer, D.; Sachse, G. W.; Sessions, W.; Weber, R. J.; Weinheimer, A. J.; Wisthaler, A.; Jimenez, J. L., Effects of aging on organic aerosol from open biomass burning smoke in aircraft and laboratory studies. *Atmos. Chem. Phys.* **2011,** *11*, (23), 12049-12064.
41. Lee, T.; Sullivan, A. P.; Mack, L.; Jimenez, J. L.; Kreidenweis, S. M.; Onasch, T. B.; Worsnop, D. R.; Malm, W.; Wold, C. E.; Hao, W. M.; Collett, J. L., Chemical Smoke Marker Emissions During Flaming and Smoldering Phases of Laboratory Open Burning of Wildland Fuels. *Aerosol Science and Technology* **2010,** *44*, (9), i-v.
42. May, A. A.; Levin, E. J. T.; Hennigan, C. J.; Riipinen, I.; Lee, T.; Collett, J. L.; Jimenez, J. L.; Kreidenweis, S. M.; Robinson, A. L., Gas-particle partitioning of primary organic aerosol emissions: 3. Biomass burning. *Journal of Geophysical Research: Atmospheres* **2013,** *118*, (19), 2013JD020286.
43. Zhou, S.; Collier, S. C.; Jaffe, D. A.; Briggs, N. L.; Hee, J.; Sedlacek III, A. J.; Kleinman, L.; Zhang, Q., Influence of Wildfires on Aerosol Chemistry in the Western US and Insights into Atmospheric Aging of Biomass Burning Organic Aerosol: Results from Mt. Bachelor Observatory (2763 m a.s.l.) during the BBOP campaign. *Atmos. Chem. Phys.* **2016,** *In Preparation*.
44. Ortega, A. M.; Day, D. A.; Cubison, M. J.; Brune, W. H.; Bon, D.; de Gouw, J. A.; Jimenez, J. L., Secondary organic aerosol formation and primary organic aerosol oxidation from biomass-burning smoke in a flow reactor during FLAME-3. *Atmos. Chem. Phys.* **2013,** *13*, (22), 11551-11571.

45. Hennigan, C. J.; Miracolo, M. A.; Engelhart, G. J.; May, A. A.; Presto, A. A.; Lee, T.; Sullivan, A. P.; McMeeking, G. R.; Coe, H.; Wold, C. E.; Hao, W. M.; Gilman, J. B.; Kuster, W. C.; de Gouw, J.; Schichtel, B. A.; Collett, J. L.; Kreidenweis, S. M.; Robinson, A. L., Chemical and physical transformations of organic aerosol from the photo-oxidation of open biomass burning emissions in an environmental chamber. *Atmospheric Chemistry and Physics* **2011,** *11*, (15), 7669-7686.
46. Grieshop, A. P.; Donahue, N. M.; Robinson, A. L., Laboratory investigation of photochemical oxidation of organic aerosol from wood fires 2: analysis of aerosol mass spectrometer data. *Atmos. Chem. Phys.* **2009,** *9*, (6), 2227-2240.
47. Vakkari, V.; Kerminen, V.-M.; Beukes, J. P.; Tiitta, P.; van Zyl, P. G.; Josipovic, M.; Venter, A. D.; Jaars, K.; Worsnop, D. R.; Kulmala, M.; Laakso, L., Rapid changes in biomass burning aerosols by atmospheric oxidation. *Geophysical Research Letters* **2014,** *41*, (7), 2644-2651.
48. Capes, G.; Johnson, B.; McFiggans, G.; Williams, P. I.; Haywood, J.; Coe, H., Aging of biomass burning aerosols over West Africa: Aircraft measurements of chemical composition, microphysical properties, and emission ratios. *Journal of Geophysical Research: Atmospheres* **2008,** *113*, (D23), D00C15.
49. Jolleys, M. D.; Coe, H.; McFiggans, G.; Taylor, J. W.; O'Shea, S. J.; Le Breton, M.; Bauguitte, S. J. B.; Moller, S.; Di Carlo, P.; Aruffo, E.; Palmer, P. I.; Lee, J. D.; Percival, C. J.; Gallagher, M. W., Properties and evolution of biomass burning organic aerosol from Canadian boreal forest fires. *Atmos. Chem. Phys.* **2015,** *15*, (6), 3077-3095.
50. Schneider, J.; Weimer, S.; Drewnick, F.; Borrmann, S.; Helas, G.; Gwaze, P.; Schmid, O.; Andreae, M. O.; Kirchner, U., Mass spectrometric analysis and aerodynamic properties of various types of combustion-related aerosol particles. *International Journal of Mass Spectrometry* **2006,** *258*, (1–3), 37-49.
51. Arangio, A. M.; Slade, J. H.; Berkemeier, T.; Pöschl, U.; Knopf, D. A.; Shiraiwa, M., Multiphase Chemical Kinetics of OH Radical Uptake by Molecular Organic Markers of Biomass Burning Aerosols: Humidity and Temperature Dependence, Surface Reaction, and Bulk Diffusion. *The Journal of Physical Chemistry A* **2015,** *119*, (19), 4533-4544.
52. Akagi, S. K.; Craven, J. S.; Taylor, J. W.; McMeeking, G. R.; Yokelson, R. J.; Burling, I. R.; Urbanski, S. P.; Wold, C. E.; Seinfeld, J. H.; Coe, H.; Alvarado, M. J.; Weise, D. R., Evolution of trace gases and particles emitted by a chaparral fire in California. *Atmos. Chem. Phys.* **2012,** *12*, (3), 1397-1421.
53. May, A. A.; McMeeking, G. R.; Lee, T.; Taylor, J. W.; Craven, J. S.; Burling, I.; Sullivan, A. P.; Akagi, S.; Collett, J. L.; Flynn, M.; Coe, H.; Urbanski, S. P.; Seinfeld, J. H.; Yokelson, R. J.; Kreidenweis, S. M., Aerosol emissions from prescribed fires in the United States: A synthesis of laboratory and aircraft measurements. *Journal of Geophysical Research: Atmospheres* **2014**, 2014JD021848.
54. Weimer, S.; Alfarra, M.; Schreiber, D.; Mohr, M.; Prévôt, A.; Baltensperger, U., Organic aerosol mass spectral signatures from wood‐burning emissions: Influence of burning conditions and wood type. *Journal of Geophysical Research: Atmospheres* **2008,** *113*, (D10).
55. Hecobian, A.; Liu, Z.; Hennigan, C. J.; Huey, L. G.; Jimenez, J. L.; Cubison, M. J.; Vay, S.; Diskin, G. S.; Sachse, G. W.; Wisthaler, A.; Mikoviny, T.; Weinheimer, A. J.; Liao, J.; Knapp, D. J.; Wennberg, P. O.; Kürten, A.; Crounse, J. D.; Clair, J. S.; Wang, Y.; Weber, R. J., Comparison of chemical characteristics of 495 biomass burning plumes intercepted by the NASA DC-8 aircraft during the ARCTAS/CARB-2008 field campaign. *Atmos. Chem. Phys.* **2011,** *11*, (24), 13325-13337.

56. Kroll, J. H.; Donahue, N. M.; Jimenez, J. L.; Kessler, S. H.; Canagaratna, M. R.; Wilson, K. R.; Altieri, K. E.; Mazzoleni, L. R.; Wozniak, A. S.; Bluhm, H.; Mysak, E. R.; Smith, J. D.; Kolb, C. E.; Worsnop, D. R., Carbon oxidation state as a metric for describing the chemistry of atmospheric organic aerosol. *Nat Chem* **2011,** *3*, (2), 133-139.
57. Zhang, Q.; Alfarra, M. R.; Worsnop, D. R.; Allan, J. D.; Coe, H.; Canagaratna, M. R.; Jimenez, J. L., Deconvolution and Quantification of Hydrocarbon-like and Oxygenated Organic Aerosols Based on Aerosol Mass Spectrometry. *Environmental Science & Technology* **2005,** *39*, (13), 4938-4952.
58. Heringa, M. F.; DeCarlo, P. F.; Chirico, R.; Lauber, A.; Doberer, A.; Good, J.; Nussbaumer, T.; Keller, A.; Burtscher, H.; Richard, A.; Miljevic, B.; Prevot, A. S. H.; Baltensperger, U., Time-Resolved Characterization of Primary Emissions from Residential Wood Combustion Appliances. *Environmental Science & Technology* **2012,** *46*, (20), 11418-11425.
59. Heringa, M. F.; DeCarlo, P. F.; Chirico, R.; Tritscher, T.; Dommen, J.; Weingartner, E.; Richter, R.; Wehrle, G.; Prévôt, A. S. H.; Baltensperger, U., Investigations of primary and secondary particulate matter of different wood combustion appliances with a high-resolution time-of-flight aerosol mass spectrometer. *Atmos. Chem. Phys.* **2011,** *11*, (12), 5945-5957.
60. Jolleys, M. D.; Coe, H.; McFiggans, G.; McMeeking, G. R.; Lee, T.; Kreidenweis, S. M.; Collett, J. L.; Sullivan, A. P., Organic aerosol emission ratios from the laboratory combustion of biomass fuels. *Journal of Geophysical Research: Atmospheres* **2014,** *119*, (22), 12,850-12,871.
61. May, A. A.; Lee, T.; McMeeking, G. R.; Akagi, S.; Sullivan, A. P.; Urbanski, S.; Yokelson, R. J.; Kreidenweis, S. M., Observations and analysis of organic aerosol evolution in some prescribed fire smoke plumes. *Atmos. Chem. Phys. Discuss.* **2015,** *15*, (2), 1953-1988.
62. Alves, C. A.; Vicente, A.; Monteiro, C.; Gonçalves, C.; Evtyugina, M.; Pio, C., Emission of trace gases and organic components in smoke particles from a wildfire in a mixed-evergreen forest in Portugal. *Science of The Total Environment* **2011,** *409*, (8), 1466-1475.
63. Christian, T. J.; Kleiss, B.; Yokelson, R. J.; Holzinger, R.; Crutzen, P. J.; Hao, W. M.; Saharjo, B. H.; Ward, D. E., Comprehensive laboratory measurements of biomass-burning emissions: 1. Emissions from Indonesian, African, and other fuels. *Journal of Geophysical Research: Atmospheres* **2003,** *108*, (D23), 4719.
64. Ward, D. E.; Hardy, C. C., Smoke emissions from wildland fires. *Environment International* **1991,** *17*, (2–3), 117-134.

Tables

Table 1: Summary of measured aerosol enhancement parameter statistics divided into smoldering (MCE < 0.9), flaming (MCE > 0.9) and all conditions for the 32 plumes measured at MBO and from G-1. The division between smoldering and flaming regimes is defined as MCE = 0.9, at which point an equal amount of smoldering and flaming combustion is present[16, 64]. Errors represent SD and number of independent data points, N = 16 and 16 for smoldering and flaming respectively.

		Smoldering			Flaming			All		
		Mean		St Dev	Mean		St Dev	Mean		St Dev
MCE		0.87	±	0.024	0.94	±	0.029	0.91	±	0.046
$fC_2H_4O_2$		0.018	±	0.0039	0.012	±	0.0061	0.015	±	0.0058
fC_4H_9		0.012	±	0.0029	0.010	±	0.0036	0.011	±	0.0033
H/C		1.7	±	0.056	1.6	±	0.098	1.6	±	0.084
O/C		0.47	±	0.078	0.57	±	0.16	0.52	±	0.13
OSc		-0.71	±	0.20	-0.46	±	0.41	-0.59	±	0.34
OM/OC		1.8	±	0.10	1.9	±	0.20	1.8	±	0.17
$\Delta NH_4/\Delta\Sigma C$	$\mu gm^{-3}/ppm_v$	0.47	±	0.38	0.17	±	0.092	0.32	±	0.32
$\Delta NO_3/\Delta\Sigma C$	$\mu gm^{-3}/ppm_v$	1.2	±	1.2	0.40	±	0.32	0.81	±	0.94
$\Delta Org/\Delta\Sigma C$	$\mu gm^{-3}/ppm_v$	46	±	25	17	±	10	31	±	24
$\Delta Org/\Delta CO$	$\mu gm^{-3}/ppb_v$	0.33	±	0.098	0.26	±	0.046	0.30	±	0.084
$\Delta OC/\Delta\Sigma C$	gC/gC	0.049	±	0.028	0.017	±	0.010	0.033	±	0.026
$\Delta Sct/\Delta\Sigma C$ *	Mm^{-1}/ppm_v	155	±	48	57	±	38	109	±	66

*Scattering enhancement averages are for MBO data only

Figures

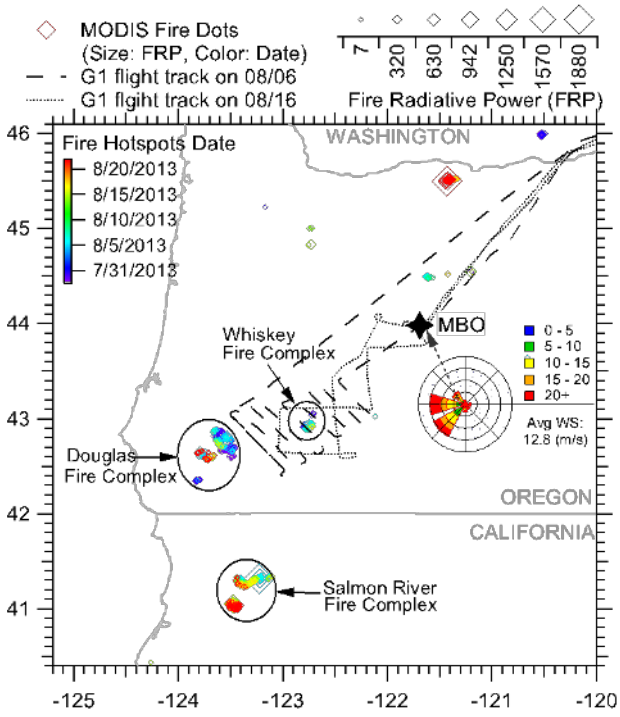

Figure 1: Map of the Pacific Northwest U.S. with the location of MBO and two G-1 aircraft flight trajectories shown. Open diamonds represent fires detected by the MODIS satellite during the period spanning the measurement campaign and are colored by date and sized by fire radiative power (FRP). Persistent and large-scale wildfires are highlighted by orange circles. The inset polar graph represents the statistical distribution of wind direction and speed at MBO during Jul. 25 – Aug. 25, 2013.

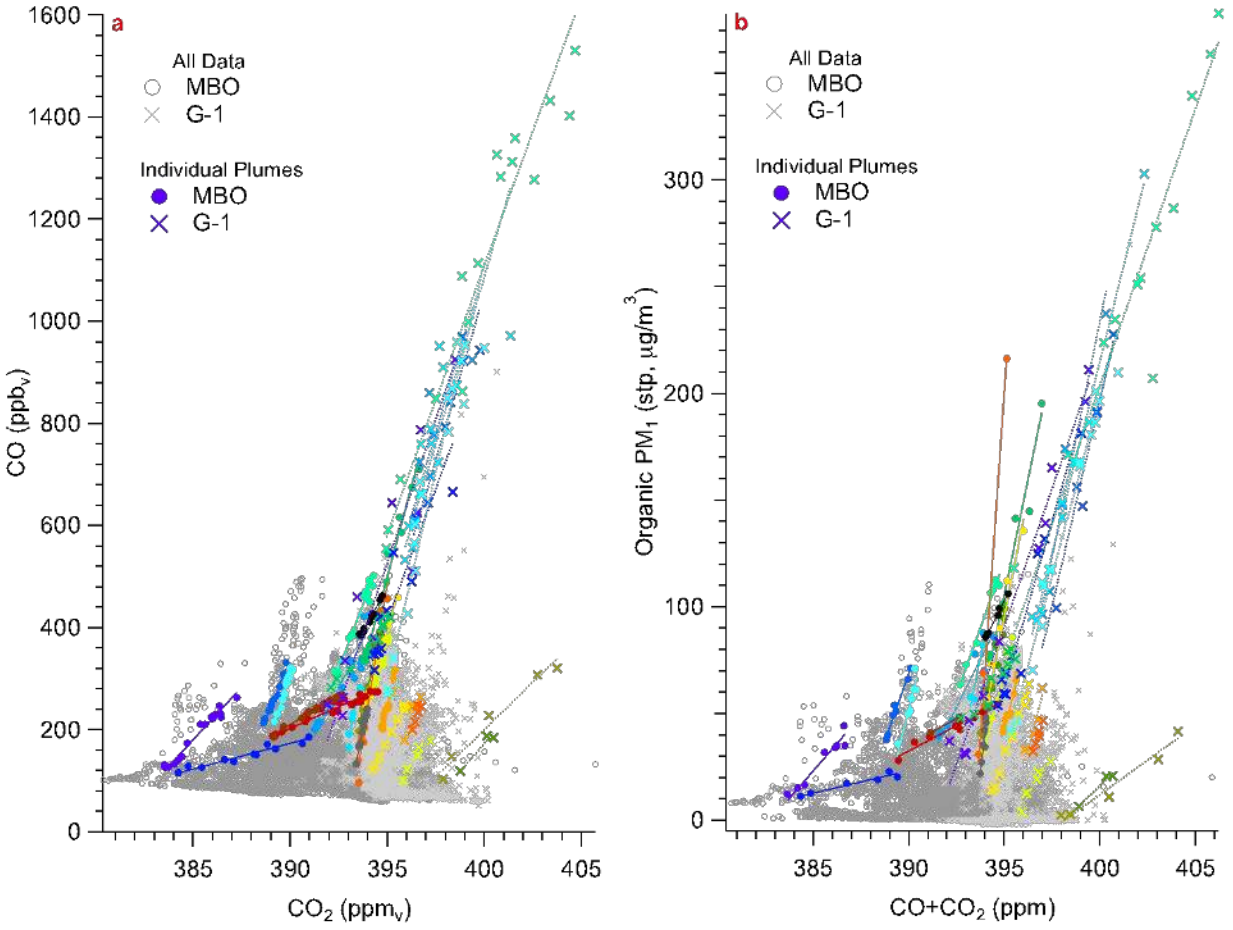

Figure 2: Scatter plots of (a) gas-phase CO vs CO_2 in ppb_v/ppm_v, and (b) particulate organics vs $CO+CO_2$ in $\mu gm^{-3}/ppm_v$. Enhancement ratios for individual plumes measured at MBO and by the G-1 aircraft are highlighted by colored markers and individual Pearson's r^2, slope and intercepts are summarized in Table S2.

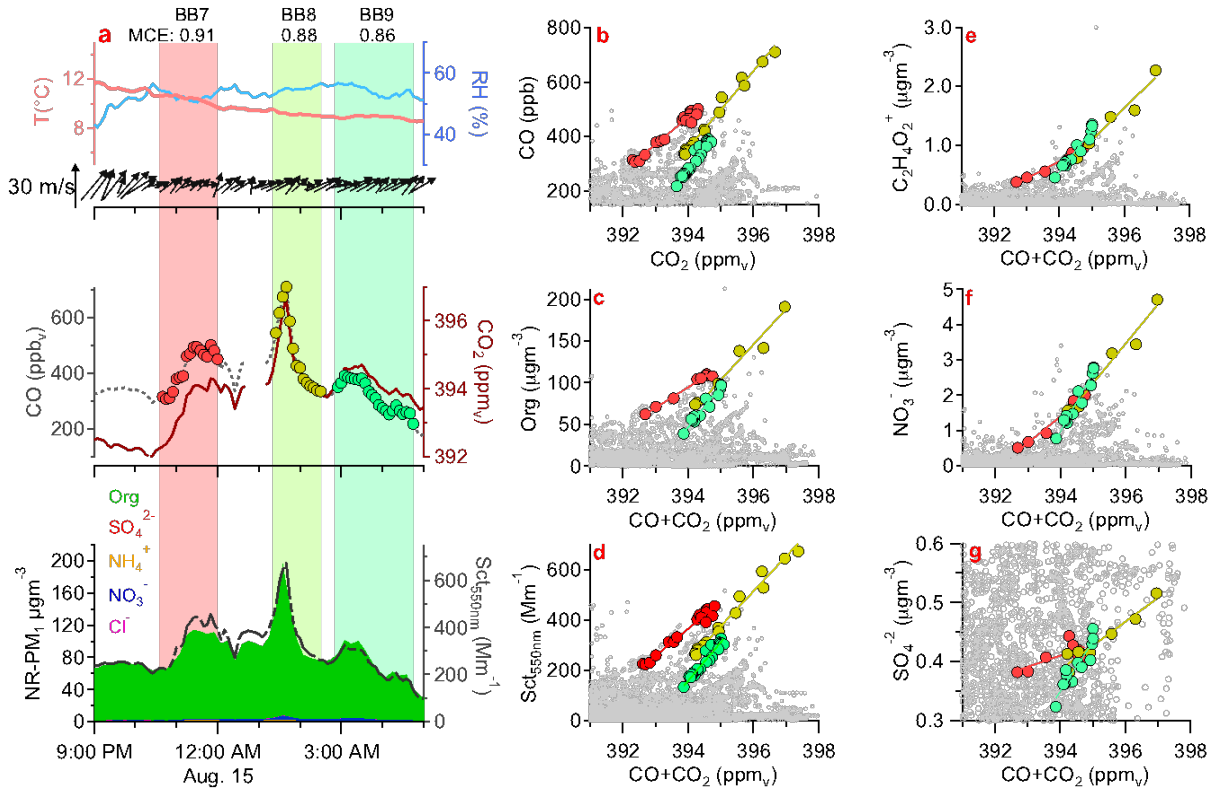

Panel		b		c		d		e		f		g	
ID	MCE	CO (ppb_v) vs CO_2 (ppm_v)		Org (μgm^{-3}) vs $CO+CO_2$ (ppm_v)		Sct_{550nm} (Mm^{-1}) vs $CO+CO_2$ (ppm_v)		$C_2H_4O_2$ (μgm^{-3}) vs $CO+CO_2$ (ppm_v)		NO_3^- (μgm^{-3}) vs $CO+CO_2$ (ppm_v)		SO_4^{2-} (μgm^{-3}) vs $CO+CO_2$ (ppm_v)	
		Slope	r^2	*Slope*	r^2	*Slope*	r^2	*Slope*	r^2	*Slope*	r^2	*Slope*	r^2
BB7	**0.91**	99 ± 4.1	0.97	25 ± 1.4	0.98	110 ± 4.9	0.97	0.28 ± 0.016	0.98	0.77 ± 0.052	0.97	0.028 ± 0.011	0.51
BB8	**0.88**	140 ± 5.2	0.98	44 ± 4.0	0.96	140 ± 5.7	0.98	0.54 ± 0.047	0.96	1.2 ± 0.090	0.97	0.060 ± 0.0074	0.93
BB9	**0.86**	170 ± 8.7	0.95	50 ± 3.7	0.95	150 ± 8.6	0.94	0.72 ± 0.052	0.95	1.7 ± 0.13	0.94	0.12 ± 0.016	0.85

Figure 3: Detailed description of 3 consecutive plumes occurring during 21:00 PM 08/14/2013 to 5:00 AM 08/15/2013. (a) The time series of temperature, RH, wind direction and speed, CO and CO_2 mixing ratios, concentrations of individual NR-PM_1 species under standard conditions (shown as stacked), and total PM_1 scattering. The three plumes are highlighted with colored bars and corresponding MCE is displayed at the top of the graph. Scatter plots, with the same three plumes highlighted by the same colored markers and fit lines, as well as showing all data measured throughout campaign in grey markers are shown for (b) CO vs CO_2 and (c - g) organic PM_1, aerosol scattering, $C_2H_4O_2^+$, nitrate and sulfate vs $CO+CO_2$. The table beneath the figures shows a summary of the slopes of the linear regressions depicted in Fig. 2b-2g and are defined here as the enhancement ratios.

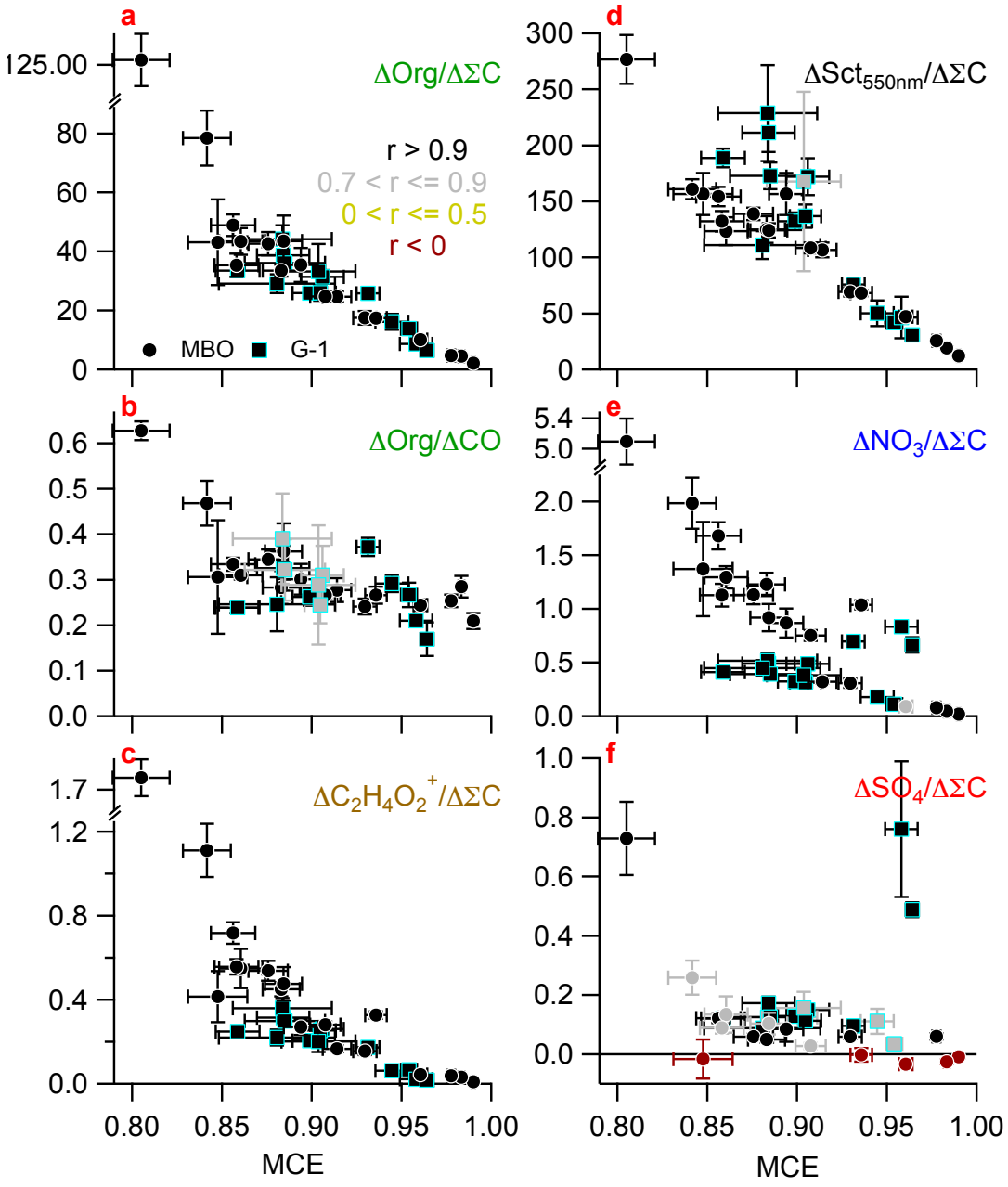

Figure 4: Enhancement ratios of (a) organic mass, (b) $C_2H_4O_2^+$, (c) $C_3H_5O_2^+$, (d) aerosol light scattering, (e) nitrate and (f) sulfate relative to $CO+CO_2$ vs MCE. ERs with respect to ΣC are in μg m^{-3}/ppm_v for Org, NO_3, and SO_4, in org-equivalent μg m^{-3}/ppm_v for $C_2H_4O_2^+$, and Mm^{-1}/ppm_v for scattering. ER of Org with respect to CO is in μg m^{-3}/ppb_v. Markers are either filled circles for MBO plumes or filled squares with a blue stroke for G-1 plumes and all are colored based on correlation coefficients between the given variable and $CO+CO_2$ or CO. Error bars for ER and MCE values represent the linear regressions errors of the calculated slopes. Note that axes are split for clarity for panels a, b, c and e.

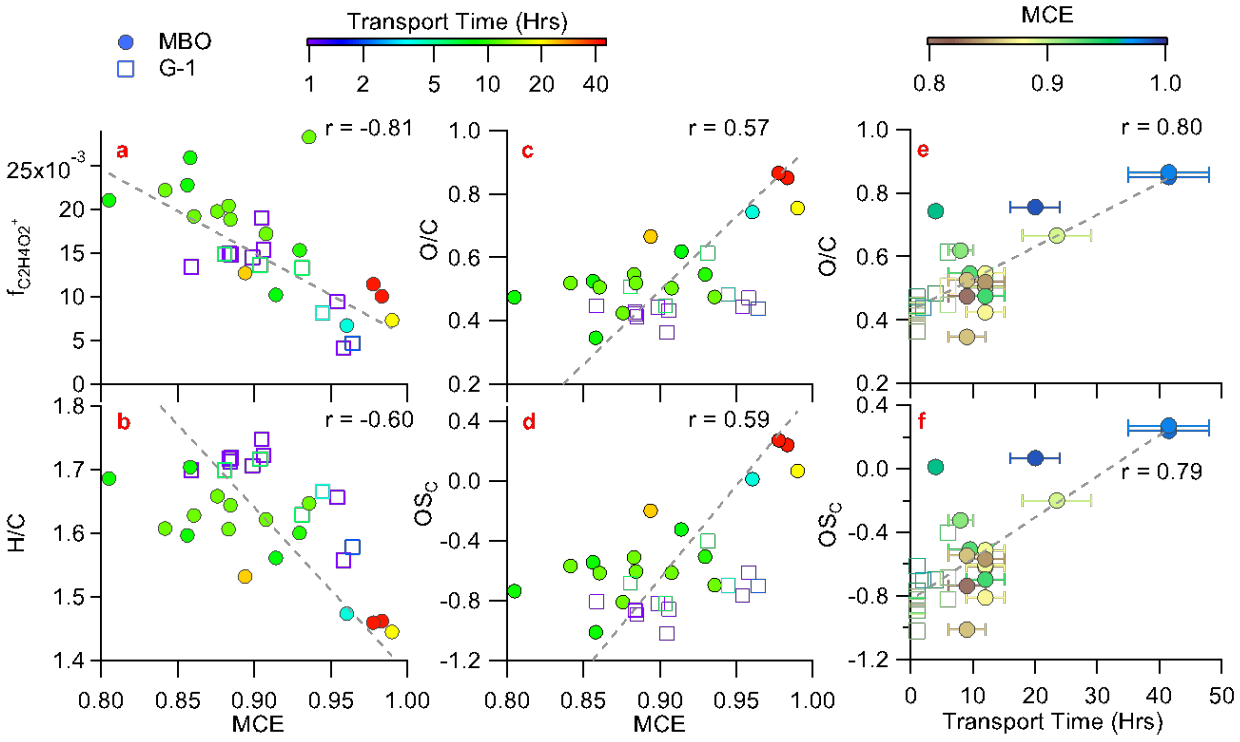

Figure 5: The parameters depicted here are derived from the ERMS calculated for each of the 32 plumes where solid circles are for MBO and open squares are for G-1. They include (a) the fractional contribution of $C_2H_4O_2^+$ to the total signal, (b) H/C, (c) O/C, and (d) OS_C vs MCE. All data points in a-d are colored by approximate transport time calculated based on HYSPLIT trajectory information. Panels e and f are the parameters O/C and OS_C, respectively, plotted vs transport time and points are colored by MCE. The Pearson's r correlation is reported in the top right panels for all parameters using least distance orthogonal fitting. The outlier in panel (a) at MCE = 0.94 and $f_{C2H4O2+}$ = 0.028 was not included in Pearson's r correlation calculation. Note that almost no correlation was observed when fitting MCE vs. Transport Time (see Fig. S24).

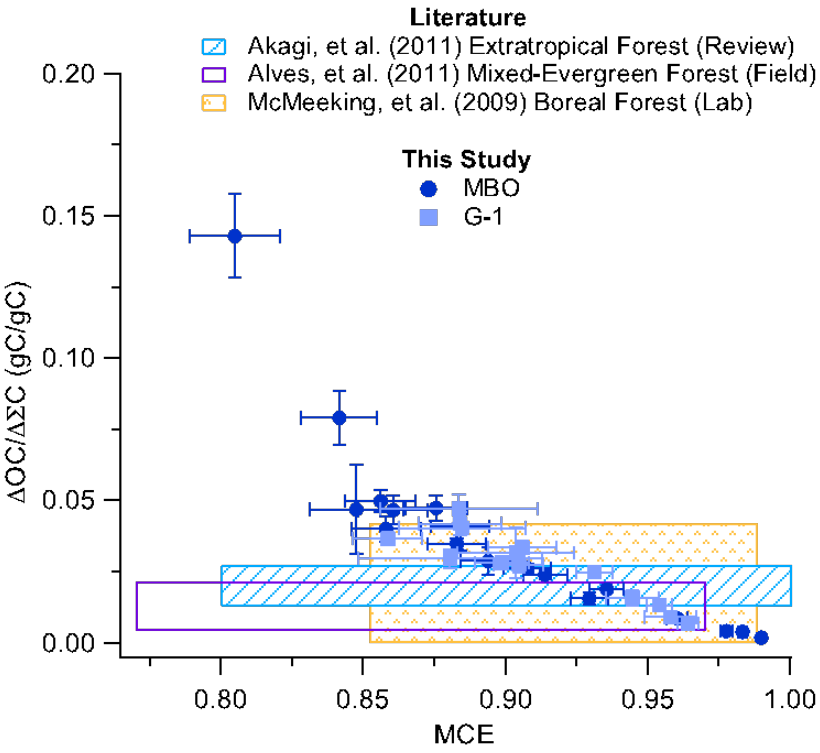

Figure 6: Emission ratio (ERs) of organic carbon determined in this study compared to ERs reported in literature using similar biomes. Error bars for ER and MCE values represent the linear regressions errors of the calculated slopes. Literature values are represented by boxes where top and bottom cover reported ER ranges and left and right sides cover reported MCE ranges. For ERs with no MCE reported the range is set to 0.8-1.0.

677 TOC Art

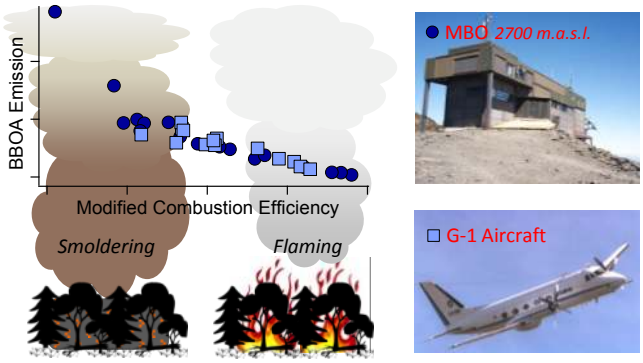

678

Supplemental Information for:

Regional Influence of Aerosol Emissions from Wildfires Driven by Combustion Efficiency: Insights from the BBOP Campaign

Sonya Collier[1], Shan Zhou[1], Timothy B. Onasch[2], Daniel A. Jaffe[3], Lawrence Kleinman[4], Arthur J. Sedlacek III[4], Nicole Briggs[5], Jonathan Hee[3], Edward Fortner[2], John E. Shilling[6], Douglas Worsnop[2], Robert J. Yokelson[7], Caroline Parworth[1], Xinlei Ge[1], Jianzhong Xu[1], Zachary Butterfield[8], Duli Chand[6], Manvendra K. Dubey[8], Mikhail Pekour[6], Stephen Springston[4], Qi Zhang[1*]

[1]Department of Environmental Toxicology, University of California, Davis, CA 95616, USA
[2]Aerodyne Research Inc., Billerica, MA 01821, USA
[3]School of Science and Technology, University of Washington, Bothell, WA 98011, USA
[4] Environmental and Climate Sciences Department, Brookhaven National Laboratory, Upton, NY 11973, USA
[5]Gradient Corporation, Seattle WA 98101, USA
[6]Atmospheric Sciences and Global Change Division, Pacific Northwest National Laboratory, Richland, WA 99352, USA
[7]Department of Chemistry, University of Montana, Missoula, MT 59812, USA
[8]Earth and Environmental Sciences Division, Los Alamos National Laboratory, Los Alamos, NM 87545, USA

*Corresponding author: Qi Zhang, dkwzhang@ucdavis.edu, (530)752-5779, Department of Environmental Toxicology, University of California, 1 Shields Ave. Davis, CA 95616

Contents

1. Methods

1.1. Measurements from Mount Bachelor Observatory (MBO)

MBO is one of the only high elevation, free tropospheric research sites in the Western U.S. It is located at the summit of Mt. Bachelor (43.9794° N, 121.6885° W, 2,763 m asl), a relatively isolated volcanic peak with few local interfering emissions and frequent sampling of tropospheric air [1-3]. MBO has been utilized for sampling air quality for 10 years. Observations have included consistent elevated spring and summer PM loadings, where spring plumes correspond to Asian long-range transport (LRT) and summer plumes are due to wildfire emissions from Oregon, California, Canada and Alaska [1, 2]. MBO is well situated for sampling wildfire emissions in the Pacific Northwest, where wildfires are a significant source of PM during summer months and one of the most active wildfire regions in the contiguous US [3-6].

1.1.1. Aerosol Mass Spectrometer

In the summer of 2013 an AMS was added to the suite of real-time continuous instruments operating at MBO as part of the BBOP campaign. The AMS has been described elsewhere [7], but briefly, the instrument inlet samples ambient air and focuses particles using an aerodynamic lens with a 1 micron size cutoff (PM_1), the focused beam is brought into a vacuum chamber where a majority of the gas-phase molecules are removed and hence particulates are concentrated up to 10^7 with respect to the gas-phase. The particle beam is modulated by a chopper wheel in 3 different positions. Open position allows all particles through, closed position blocks the particle beam and particle time-of-flight (PTOF) position allows a portion of the beam to pass at 2% duty cycle. When subtracting closed from open position signals, the ensemble mass spectra of all particles can be determined. In PTOF mode, the mass spectra of different size bins can be derived for size-resolved chemical information. The particle beam travels through a particle time-of-flight chamber and impinges on a heated porous tungsten oven where non-refractory (NR) components (organics, inorganic sulfate, nitrate, ammonium and chloride) are rapidly vaporized at 600°C. Vaporized components are ionized via electron impact (EI) at 70 eV and focused into a time-of-flight mass spectrometer (MS). The MS can be set to either V-mode or W-mode, ion optical settings for higher sensitivity or higher mass resolution, respectively.

The AMS has been used extensively for ambient and laboratory measurements of BB aerosols. For ambient sampling, factor analysis is often used to derive unique contributing

factors. BBOA factors in particular have often been identified in a variety of environments [8]. Various laboratory experiments have sought to characterize the response of the AMS to BBOA [9] and recent efforts have been made in quantifying the evolution of BBOA as a function of photochemical age, hence the AMS has been used in the FLAME series experiments at the FDA Missoula Montana Fire Lab [10].

A brief description of the AMS deployment configuration can be found in the Methods section of the main text and in Fig. S1. Ionization efficiency (IE) and relative ionization efficiency (RIE) calibrations were performed on-site at the beginning, middle, and end of the campaign using ammonium nitrate and ammonium sulfate, respectively. Particle size calibrations were performed using PSL spheres (Duke Scientific). Collection efficiency was assumed to be 0.5 since a drier was used prior to AMS sampling, which maintained low RH (< 30%) at the AMS inlet for the entire study, and organics dominated the PM composition, hence any effects from inorganic nitrate or particle acidity had negligible effects on CE [11]. In addition, particle-free ambient air was sampled at different times throughout the campaign to calculate limits of detection (LOD) for the 5 NR species (sulfate, nitrate, ammonium, chloride, and organics).

All AMS data collected at MBO was analyzed in SQ:ToF-AMS Analysis Toolkit 1.53 and PIKA:ToF-AMS HR Analysis 1.12 (downloaded from http://cires.colorado.edu/jimenez-group/ToFAMSResources/ToFSoftware/index.html), open source data analysis toolkits programmed in Igor Pro 6.34A (Wavemetrics, Inc.). Inorganic species, i.e. nitrate, sulfate, ammonium and chloride, we used high mass resolution data to directly quantify corresponding ions. Organics were quantified from unit mass resolution data but there was very high correlation and a slope of nearly 1:1 between the high resolution organic mass and that of unit mass resolution.787 individual high resolution ions were fit in PIKA, enabling elemental analysis of the averaged mass spectra for different periods or plumes to be reported. The elemental ratios of a given mass spectrum were calculated using the Improved Ambient method reported in Canagaratna, et al. [12].

An SMPS was deployed at MBO during the campaign but due to instrument malfunction, aerosol volume information was not available for comparison with the HR-AMS mass concentration. The AMS total (NR-PM_1) was compared to submicron aerosol scattering at the wavelength of 550nm (σ_{sp}). Tight correlation with $r^2 = 0.93$ was observed. The slope of the orthogonal fitting for σ_{sp} versus NR-PM_1 is 3.3 $m^2\ g^{-1}$, which is an estimate of the average dry

mass scattering efficiency (DMSE) for PM_1, given that the nephelometer measures aerosol scattering and the AMS measures non-refractory PM. This value is within the range for fine mode mixed composition aerosols (3.6±1.2 m^2 g^{-1}) [13]. Typically HR-AMS quantification of the mass concentration of NR-PM_1 species has an upper limit in uncertainty of ±30%, with the precisions in the ratio between species, elemental ratios (O/C, H/C, OM/OC, N/C), and fractional contributions of individual ions being much reduced [14].

1.1.2 Nephelometer

A TSI 3563 3-wavelength Integrating Nephelometer was used continuously throughout the measurement campaign. For this work we used data from the green channel only (550 nm). The instrument is calibrated with pure CO_2 bimonthly and the minimum detection limit is 0.4 Mm^{-1} at 550 nm. See Fischer, et al. [15] for information on calibration and typical setup of this instrument. All scattering data was converted to standard temperature and pressure.

1.1.3 Gas-phase Measurements

CO and CO_2 were measured using a Picarro G2502 Cavity Ring-Down Spectrometer. Calibrations were performed every 8 hours with a series of calibration gases referenced to the World Meteorological Organization's scale. The 1-sigma precision of 5-minute averages was approximately 1.0 ppbv for CO and 0.1 ppmv for CO_2 [16]. All data is reported in relative concentration (ppm by volume). Throughout the campaign 5-minute data was available. See McClure, et al. [17] for more details.

1.2 Measurements from the Gulfstream-1 (G-1) aircraft

During the BBOP campaign, a G-1 research aircraft of the DOE Atmospheric Radiation Measurement (ARM) Aerial Facility was used to sample the smoke-filled skies from June through October 2013. A total of 21 research flights were logged during that time span. The G-1 has a 15.3 m^2 cabin space, with 8 external probes and has a maximum endurance with full payload of 4-5 hours. Cabin payload weight was limited to 1,900 kg. The aircraft housed various online gas and particle phase sampling instruments including H_2O, CO, CO_2, CH_4, N_2O, NO, NO_2, NO_y, O_3 and SO_2 for trace gas measurements and total concentration, size distribution, cloud condensation nuclei concentration, optical properties and physico-chemical composition of aerosols. Furthermore, various radiative and meteorological parameters were measured. More

information can be found at http://www.arm.gov/campaigns/bbop/ and a full list of instrumentation can be found at http://www.arm.gov/campaigns/bbop/measurements.

1.2.1 Soot Particle Aerosol Mass Spectrometer (SP-AMS)

A Soot Particle Aerosol Mass Spectrometer (SP-AMS) and a Cavity Attenuated Phase Shift Extinction Monitor (CAPS PM_{EX}) were deployed on the G-1 to characterize the mass, chemistry, optical properties (extinction), and size of black carbon-containing particles (laser vaporizer) and nonrefractory biomass burning particles (heated tungsten vaporizer) as they are generated in biomass burning events and as they evolve in the atmosphere. This deployment represents the first research flights for both of these instruments. For this study, we focus only on the nonrefractory biomass burning particle measurements obtained using the SP-AMS using the heated tungsten vaporizer (laser vaporizer was off). For more details on the deployment configuration, see the Methods section in the main text. Filter measurements were performed on every flight during the return leg. A collection efficiency of 0.5 was assumed for all particles for similar reasons as discussed above for the HR-AMS. The IE and RIE values determined from data processing are shown in Table S1 below.

1.2.2 Nephelometer

A three-wavelength integrating nephelometer (TSI Model 3563) is used at a volumetric flow of about 30 lpm to measure total and back scattering light coefficients. The covered wavelengths are at 450 nm (blue), 550 nm (green) and 700 nm (red) at 1 Hz time resolution. Stainless steel and copper tubes of 1 inch or bigger diameters are used to avoid any losses of particles in sampling lines. The air sample was slightly heated at inlet of the instrument to maintain a low relative humidity. The mean RH was below 20% most of time so that the scattering and backscatter were determined for essentially dry aerosol. The instrument was calibrated each time during the campaign period using particle free air, carbon dioxide and sulfur hexafluoride gases with a purity better than 99.99%. Since heavy smoke from forest fires were sampled by this instrument, the performance and sensitivity of the instrument was checked in starting and end of each flight. The Calibration and truncation corrections to scattering coefficients were applied as per Anderson and Ogren [18].

2. Data Analysis

2.1 Plume selection and overlap with related study

Briggs, et al. [16] conducted a study, in which various plumes from the summer of 2012 and 2013 were sampled at MBO and selected for calculation of the modified combustion efficiency. In that study the authors use a multiple-background enhancement ratio calculation method. Four plumes selected in that study overlap with plumes selected in the present study. In the Briggs, et al. [16] paper plumes 18, 21, and 23 overlap approximately with plumes 3, 8 and 15 of this study. In the present study plumes 10 and 17 are consecutive and plume 22 in Briggs, et al. [16] overlaps both of these plumes. The MCE for plumes 18, 21, 22 and 23 in Briggs, et al. [16] are calculated as 0.89±0.09, 0.92±0.09, 0.97±0.14, and 0.98±0.32 respectively. In this study the overlapping plumes have MCE of 0.92±0.0046, 0.88±0.0039, 0.86±0.0084 & 0.84±0.0058, and 0.98±0.00085 for plumes 3, 8, 10 & 17 and 15 respectively. There is reasonable overlap among plumes. Differences occur because of the different criteria used to select starting and ending points of plumes as well as the different methods in accounting for background levels of CO and CO_2. Furthermore, back trajectory analysis of these particular plumes led both studies to draw similar conclusions regarding transport time and source location. For instance Briggs, et al. [16] estimated that plume 18 had a transport time between 14 and 34 hours and the source was in SW OR, and in this study plume 3 was estimated to have a transport time between 24 and 30 hours and was also located in SW OR. Plume 21 in Briggs, et al. [16] had an estimated transport time of 10-12 hours whereas in this study plume 8 had an approximate transport time of 12-18 hours. Both were estimated to come from NW CA. Plume 22 in Briggs, et al. [16] had an estimated transport time of 10-12 hours whereas in this study, plumes 10 and 17 had an approximate transport time of 12 hours. Both were estimated to come from NW CA. Finally, for plume 23 in Briggs, et al. [16] it was estimated to have a transport time of 25-45 hours and in this study plume 15 had an estimated transport time of 42-48. In this case the source inferred for these plumes did not match up with Briggs, et al. [16] finding that plume 23 had come from SW OR whereas in this study it was inferred that it came from NE OR. Note that the back trajectory analysis presented here for plume 15 appeared relatively ambiguous. Not all plumes had a clear source and this is partly due to errors in back trajectory analysis as well as limited frequency of satellite overpasses which provide limited information on fire hotspot occurrences.

2.2 Inter-comparison between SP-AMS and HR-AMS

On two occasions the G-1 flew over MBO during the campaign period, on August 6th and 16th at 14:30 and 13:25 (PDT) respectively. Geographical overlap lasted 7-8 minutes on both occasions. As described in the main text and earlier sections of the supplementary information, the SP-AMS aboard the G-1 was averaging at 1 second time resolution while the HR-AMS at MBO was sampling at 5 minute time resolution. Given that the flyby period was relatively brief, an instrument inter-comparison can only be done for a few HR-AMS data points. Figure S2 shows the scatter plot between AMS measured organic PM_1 (corrected to STP) vs CO gas-phase concentration (ppb_v). The periods of geographical overlap are highlighted by the filled squares. The correlation between organic and CO is consistent between G-1 and MBO on both occasions. On August 6th during G-1 overlap MBO organic aerosol concentration was measured at 47 $\mu g/m^3$ and G-1 measured 43±3.4 $\mu g/m^3$. On August 16th MBO observed 36±2.1 $\mu g/m^3$ and G-1 measured 28±2.7 $\mu g/m^3$ which falls within the overall measurement uncertainty of ±30% for AMS aerosol species mass quantification [11]. Overall agreement for other important species, such as gas phase CO, CO_2, O_3, NO_y and particulate scattering are within ±15% when comparing measurements at MBO and on G-1 during the two geographical overlap periods.

3. Figures (S1 – S24)

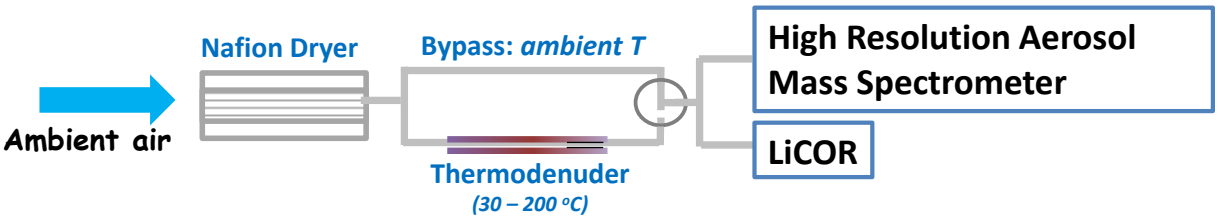

Figure S1: Schematic of instrumental setup at MBO. Ambient air was pulled in through MBO mercury inlet and dried through a Nafion dryer (PD-200T, Perma Pure LLC). Conditioned air was switched between a bypass and thermodenuder line and subsequently analyzed by both the AMS and a gas-phase LiCOR analyzer.

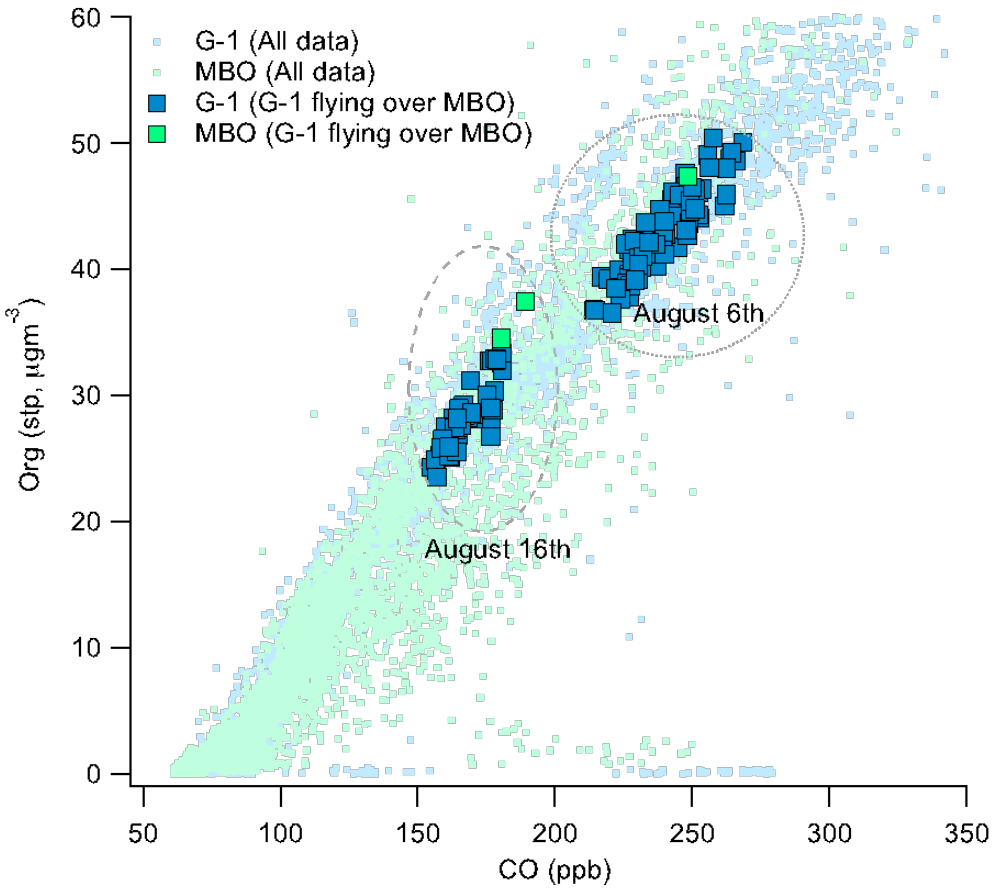

Figure S2: Scatter plot between organic PM_1 and CO for both G-1 and MBO. Periods where G-1 flew over MBO are highlighted by filled squares.

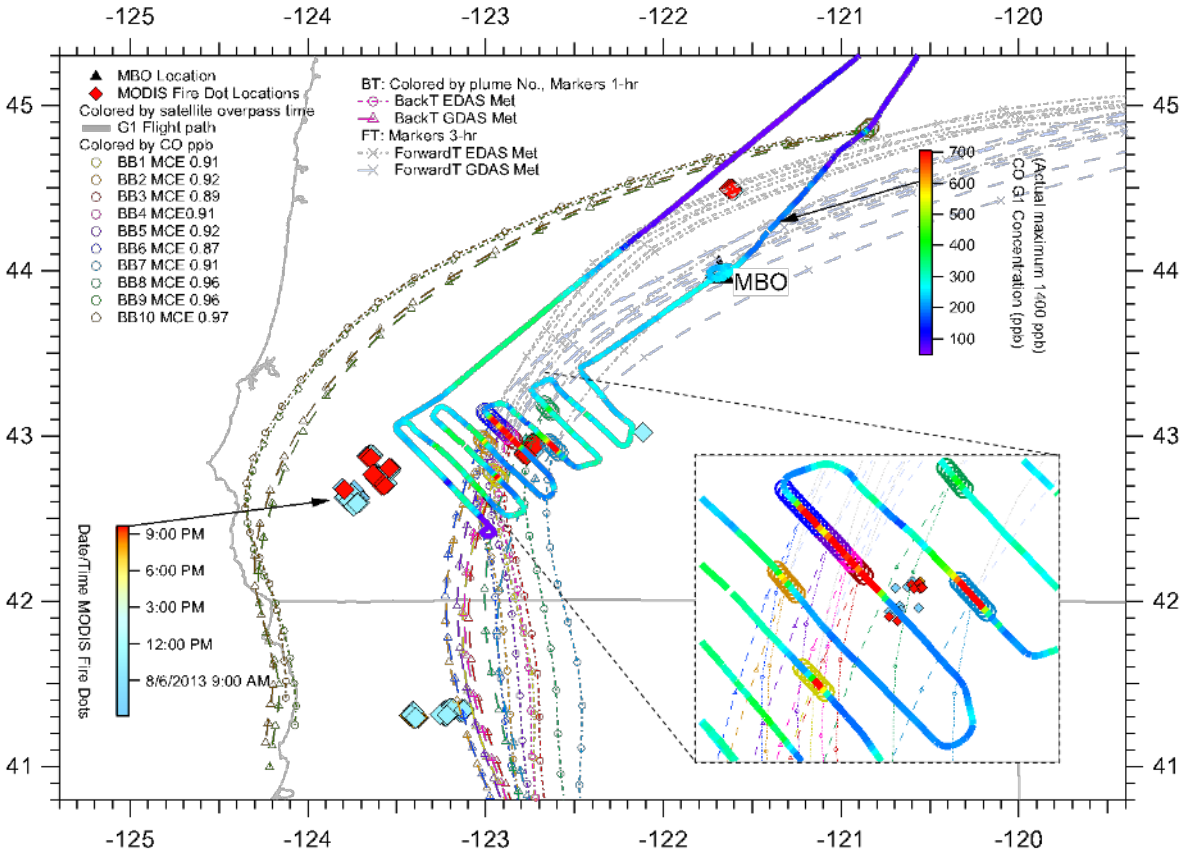

Figure S3: G-1 flight trajectory for August 6th, colored by CO concentration in ppb. G-1 Plume (August 6th) HYSPLIT 48-hour back trajectory and 48-hour forward trajectory (light blue lines and markers) analysis using high-resolution meteorological field data (GDAS) and low-resolution meteorological field data (EDAS), markers are 1-hour intervals for back trajectory and 3-hour intervals for forward trajectories. MODIS fire dot data is superimposed and colored by time (PDT). MCE for each plume ID is provided in the legend. Inset shows magnified view of transectional flight pattern.

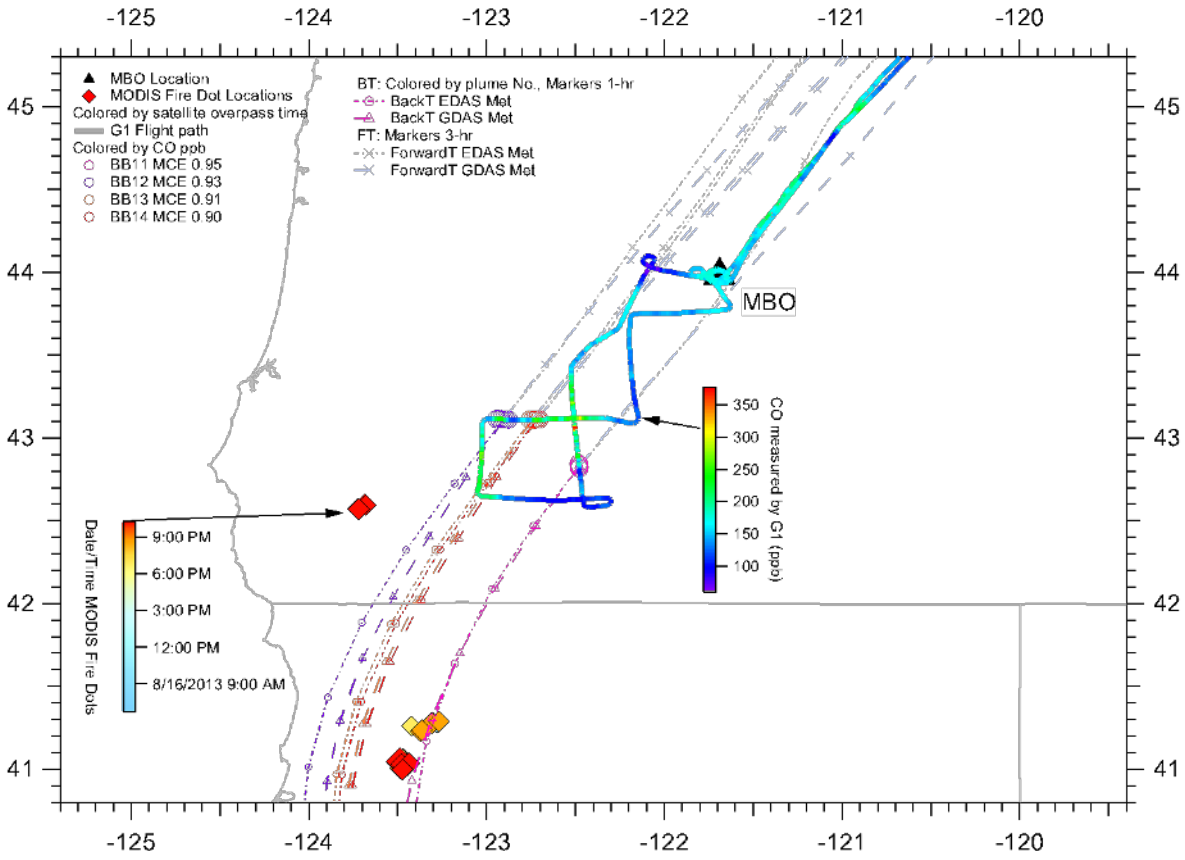

Figure S4: G-1 flight trajectory for August 16th, colored by CO concentration in ppb. G-1 Plume (August 16th) HYSPLIT 48-hour back trajectory and 48-hour forward trajectory (light blue lines and markers) analysis using high-resolution meteorological field data (GDAS) and low-resolution meteorological field data (EDAS), markers are 1-hour intervals for back trajectory and 3-hour intervals for forward trajectories. MODIS fire dot data is superimposed and colored by time (PDT). MCE for each plume ID is provided in the legend.

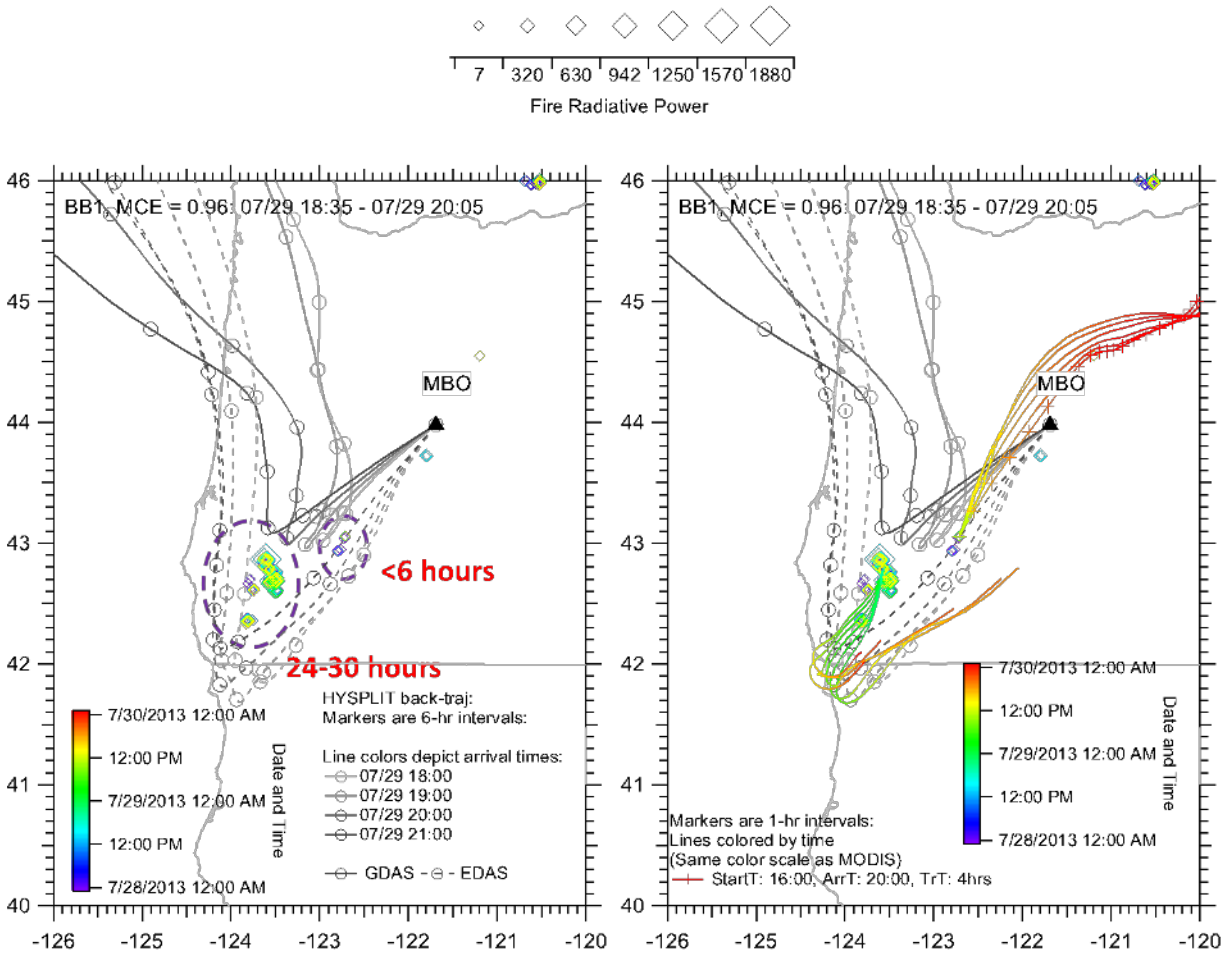

Figure S5: MBO Plume BB1 HYSPLIT 3-day back trajectory on the left and forward trajectory analysis on the right. Back trajectory uses high-resolution meteorological field data (GDAS) and low-resolution meteorological field data (EDAS), markers are 6 hour intervals and trajectories are colored by arrival date and hour (PDT). Estimated plume transport times are shown in red text and are based on back trajectory overlap with MODIS fire hotspot overlaps. Forward trajectory analyses (start times and locations based on back trajectory analysis results) use EDAS 40-km data and are colored by time (PDT) using same scale as MODIS fire hotspots. MODIS fire hotspot data is superimposed and colored by time (PDT). MCE and plume interval are provided in the top left. More refined plume transport times based on forward trajectory analyses shown in legend. Forward trajectories with markers denote trajectories where arrival time near MBO matches BB1 occurrence.

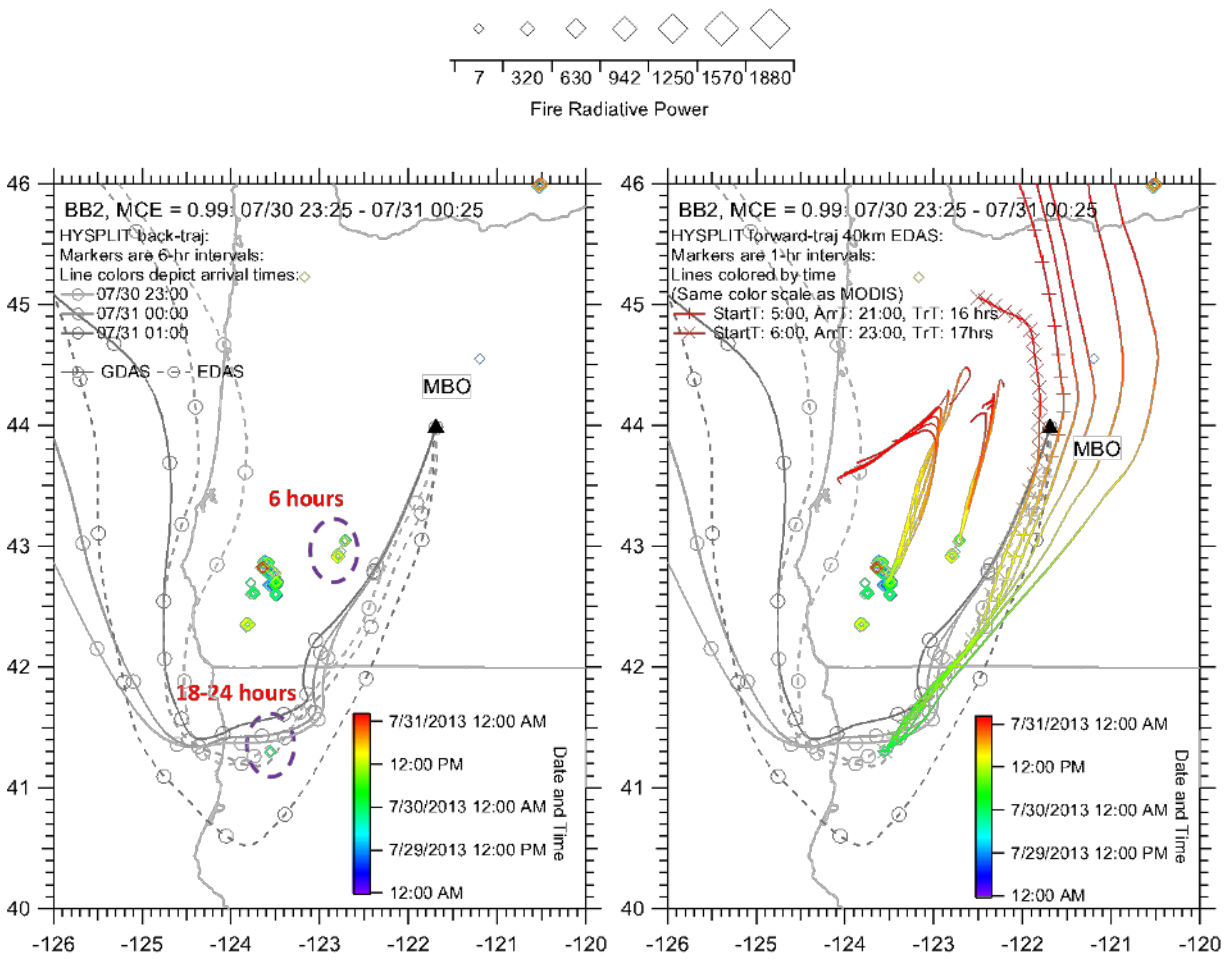

Figure S6: MBO Plume BB2 HYSPLIT 3-day back trajectory on the left and forward trajectory analysis on the right. Back trajectory uses high-resolution meteorological field data (GDAS) and low-resolution meteorological field data (EDAS), markers are 6 hour intervals and trajectories are colored by arrival date and hour (PDT). Estimated plume transport times are shown in red text and are based on back trajectory overlap with MODIS fire hotspot overlaps. Forward trajectory analyses (start times and locations based on back trajectory analysis results) use EDAS 40-km data and are colored by time (PDT) using same scale as MODIS fire hotspots. MODIS fire hotspot data is superimposed and colored by time (PDT). MCE and plume interval are provided in the top left. More refined plume transport times based on forward trajectory analyses shown in legend. Forward trajectories with markers denote trajectories where arrival time near MBO matches BB2 occurrence.

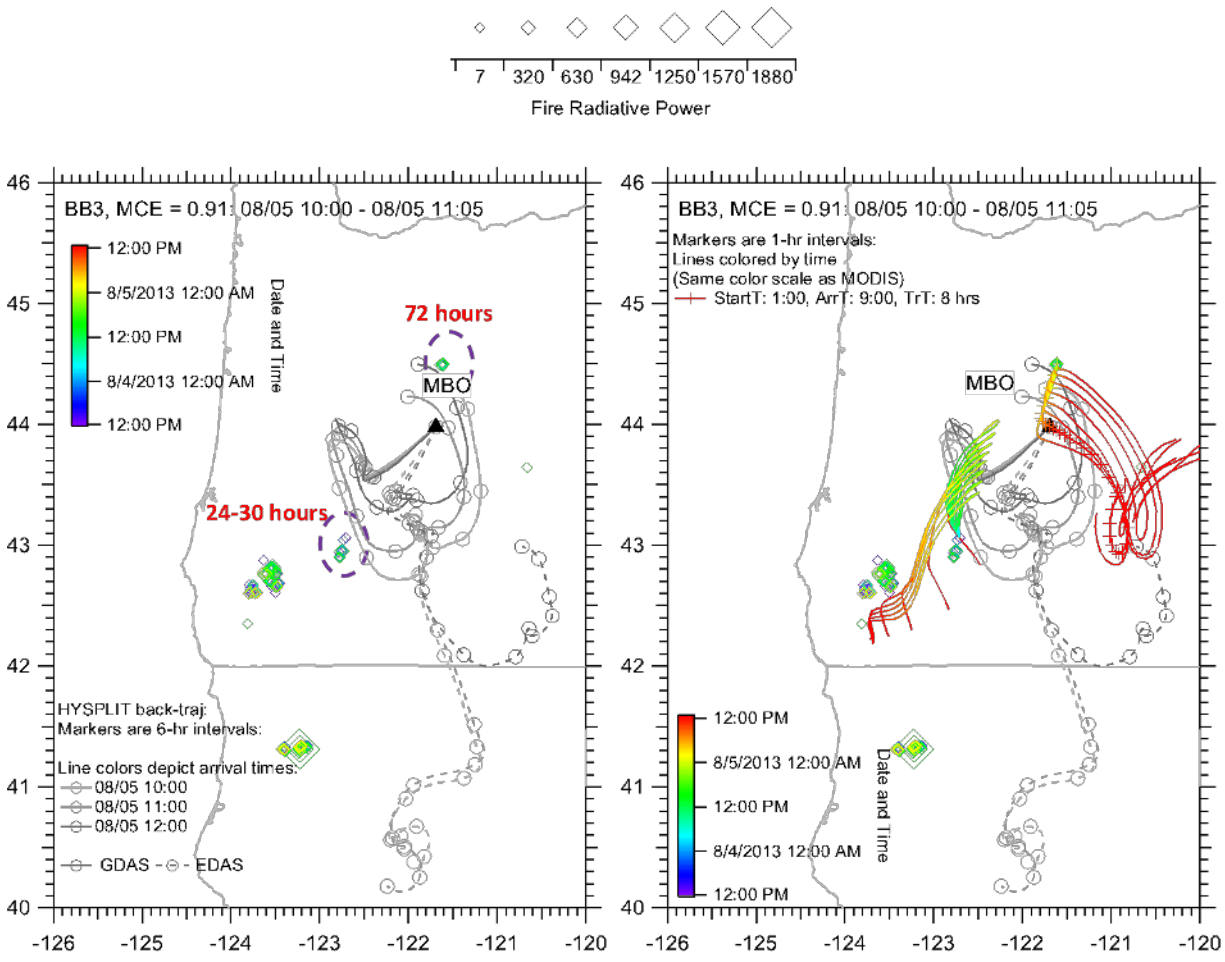

Figure S7: MBO Plume BB3 HYSPLIT 3-day back trajectory on the left and forward trajectory analysis on the right. Back trajectory uses high-resolution meteorological field data (GDAS) and low-resolution meteorological field data (EDAS), markers are 6 hour intervals and trajectories are colored by arrival date and hour (PDT). Estimated plume transport times are shown in red text and are based on back trajectory overlap with MODIS fire hotspot overlaps. Forward trajectory analyses (start times and locations based on back trajectory analysis results) use EDAS 40-km data and are colored by time (PDT) using same scale as MODIS fire hotspots. MODIS fire hotspot data is superimposed and colored by time (PDT). MCE and plume interval are provided in the top left. More refined plume transport times based on forward trajectory analyses shown in legend. Forward trajectories with markers denote trajectories where arrival time near MBO matches BB3 occurrence.

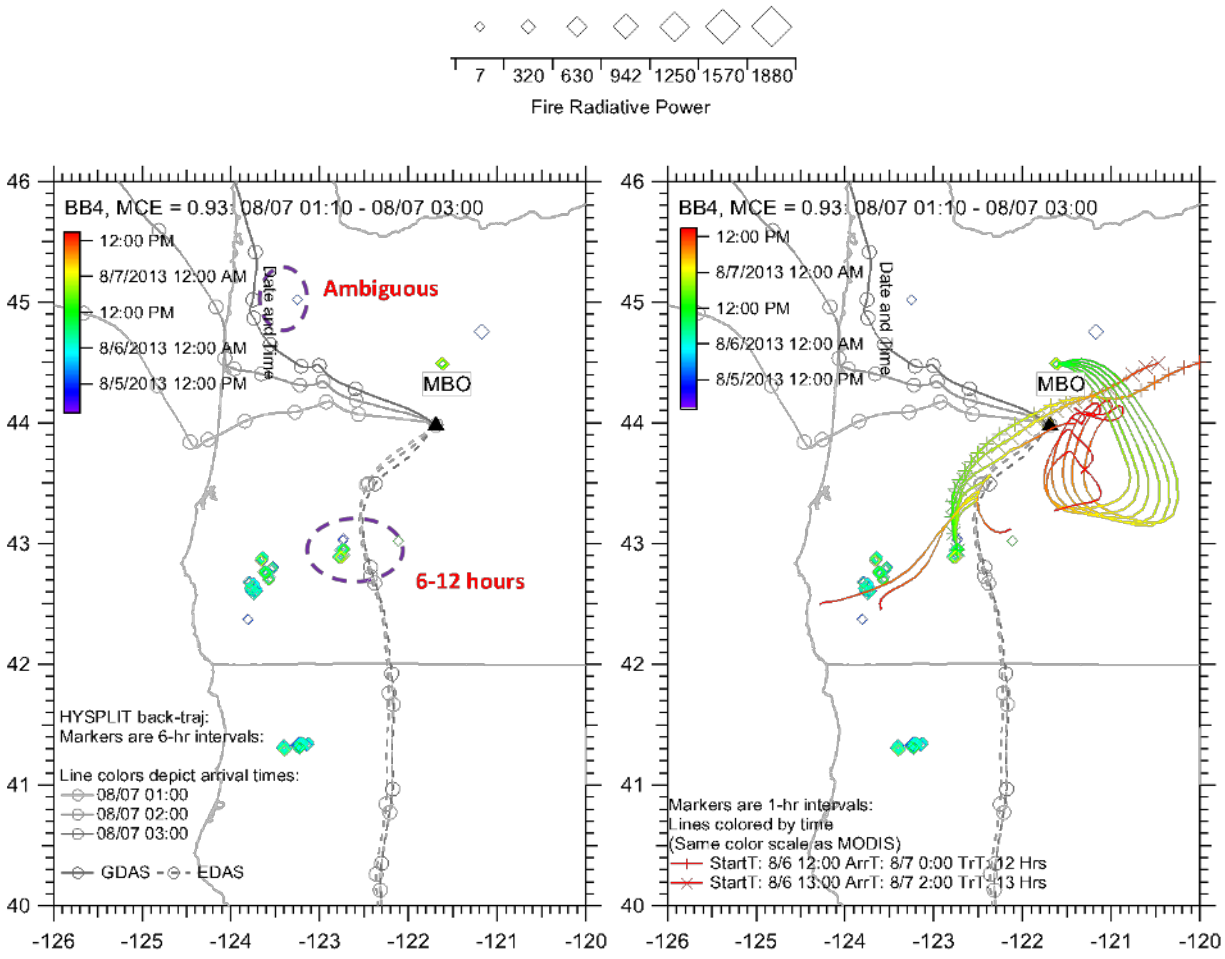

Figure S8: MBO Plume BB4 HYSPLIT 3-day back trajectory on the left and forward trajectory analysis on the right. Back trajectory uses high-resolution meteorological field data (GDAS) and low-resolution meteorological field data (EDAS), markers are 6 hour intervals and trajectories are colored by arrival date and hour (PDT). Estimated plume transport times are shown in red text and are based on back trajectory overlap with MODIS fire hotspot overlaps. Forward trajectory analyses (start times and locations based on back trajectory analysis results) use EDAS 40-km data and are colored by time (PDT) using same scale as MODIS fire hotspots. MODIS fire hotspot data is superimposed and colored by time (PDT). MCE and plume interval are provided in the top left. More refined plume transport times based on forward trajectory analyses shown in legend. Forward trajectories with markers denote trajectories where arrival time near MBO matches BB4 occurrence.

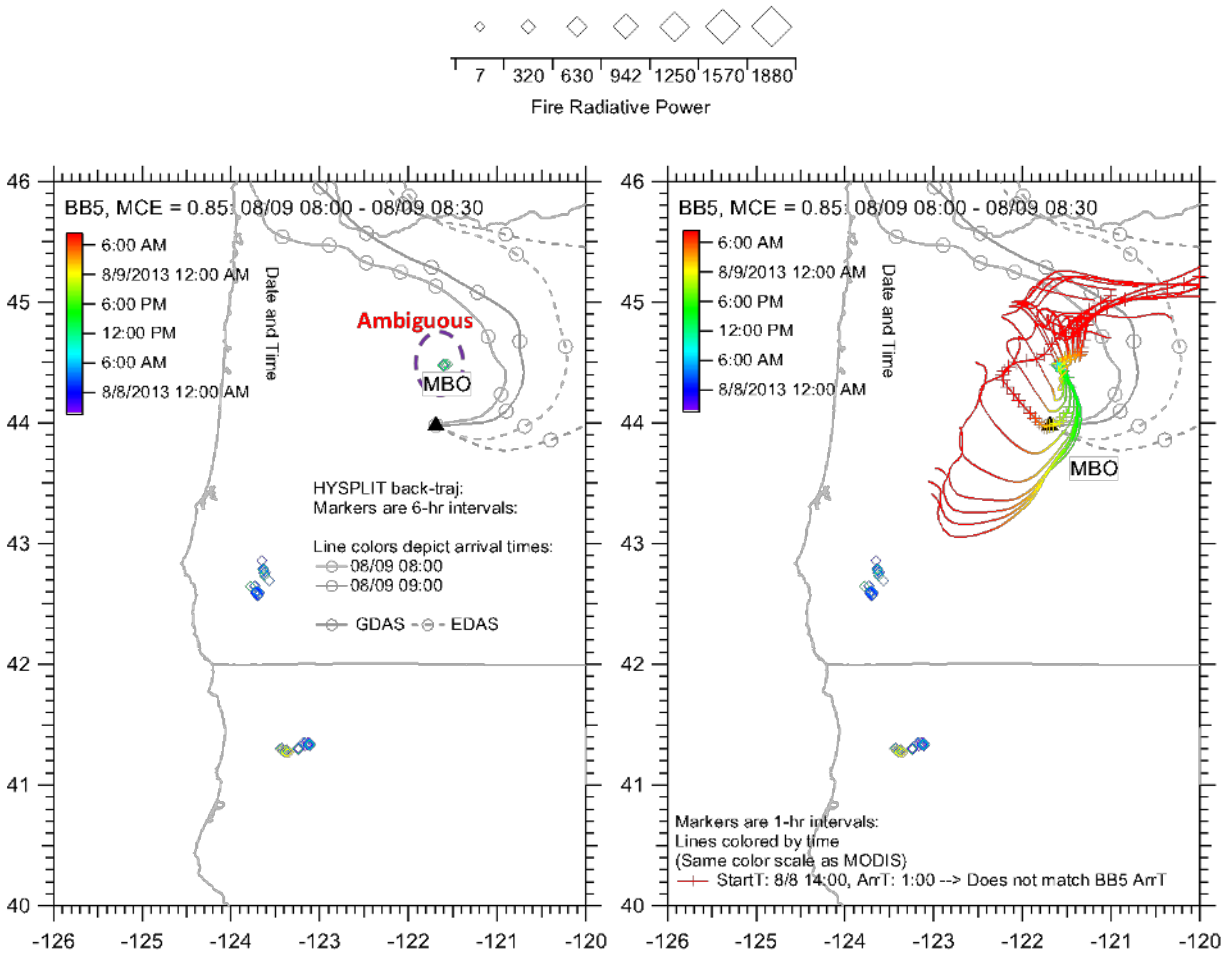

Figure S9: MBO Plume BB5 HYSPLIT 3-day back trajectory on the left and forward trajectory analysis on the right. Back trajectory uses high-resolution meteorological field data (GDAS) and low-resolution meteorological field data (EDAS), markers are 6 hour intervals and trajectories are colored by arrival date and hour (PDT). Estimated plume transport times are shown in red text and are based on back trajectory overlap with MODIS fire hotspot overlaps. Forward trajectory analyses (start times and locations based on back trajectory analysis results) use EDAS 40-km data and are colored by time (PDT) using same scale as MODIS fire hotspots. MODIS fire hotspot data is superimposed and colored by time (PDT). MCE and plume interval are provided in the top left. More refined plume transport times based on forward trajectory analyses shown in legend. Forward trajectories with markers denote trajectories where arrival time near MBO matches BB5 occurrence but for BB5 a good match was not found. It is likely that MODIS did not capture the fire which is the source of plume measured at MBO. No other sources in the Pacific Northwest area were good fits for BB5.

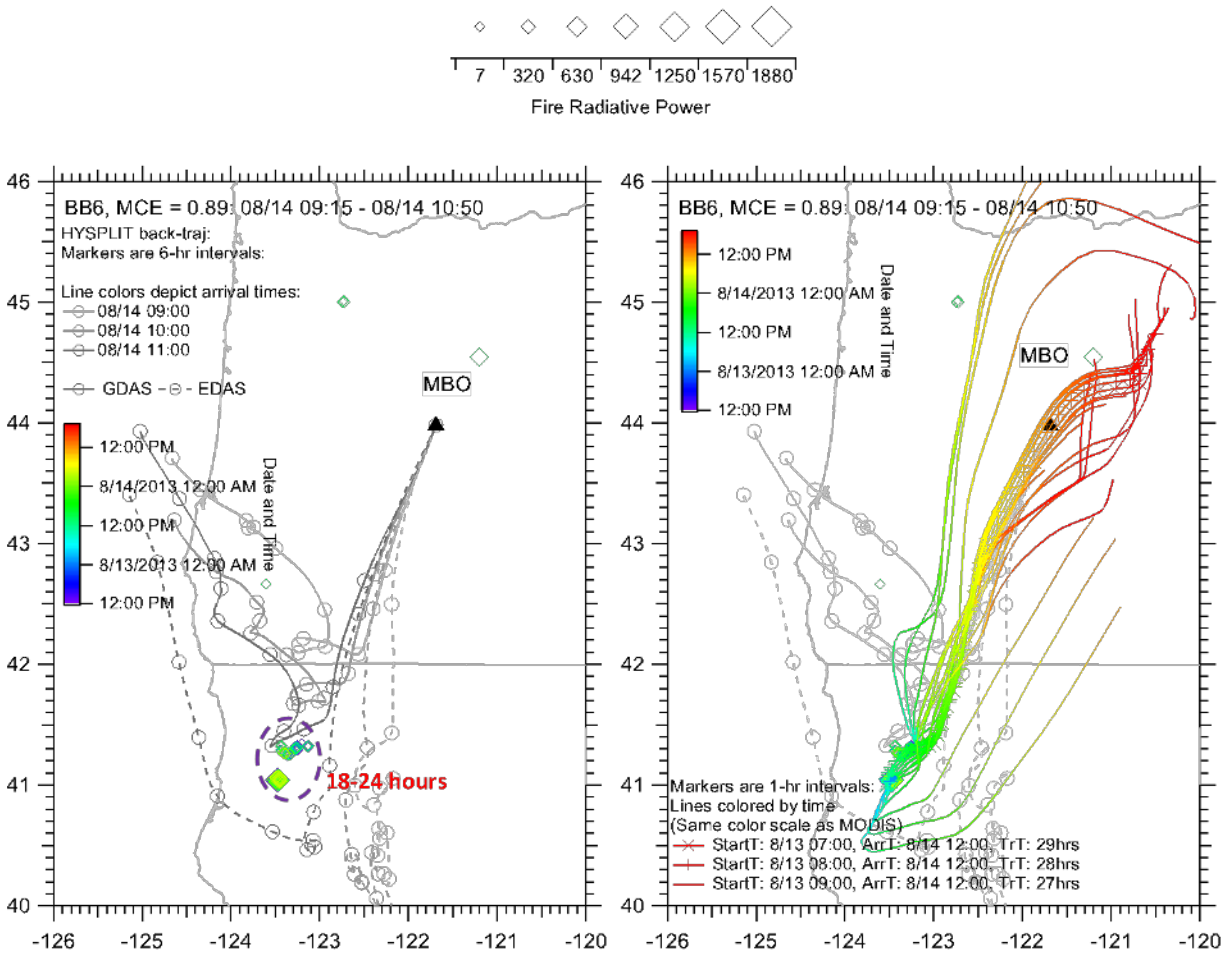

Figure S10: MBO Plume BB6 HYSPLIT 3-day back trajectory on the left and forward trajectory analysis on the right. Back trajectory uses high-resolution meteorological field data (GDAS) and low-resolution meteorological field data (EDAS), markers are 6 hour intervals and trajectories are colored by arrival date and hour (PDT). Estimated plume transport times are shown in red text and are based on back trajectory overlap with MODIS fire hotspot overlaps. Forward trajectory analyses (start times and locations based on back trajectory analysis results) use EDAS 40-km data and are colored by time (PDT) using same scale as MODIS fire hotspots. MODIS fire hotspot data is superimposed and colored by time (PDT). MCE and plume interval are provided in the top left. More refined plume transport times based on forward trajectory analyses shown in legend. Forward trajectories with markers denote trajectories where arrival time near MBO matches BB6 occurrence.

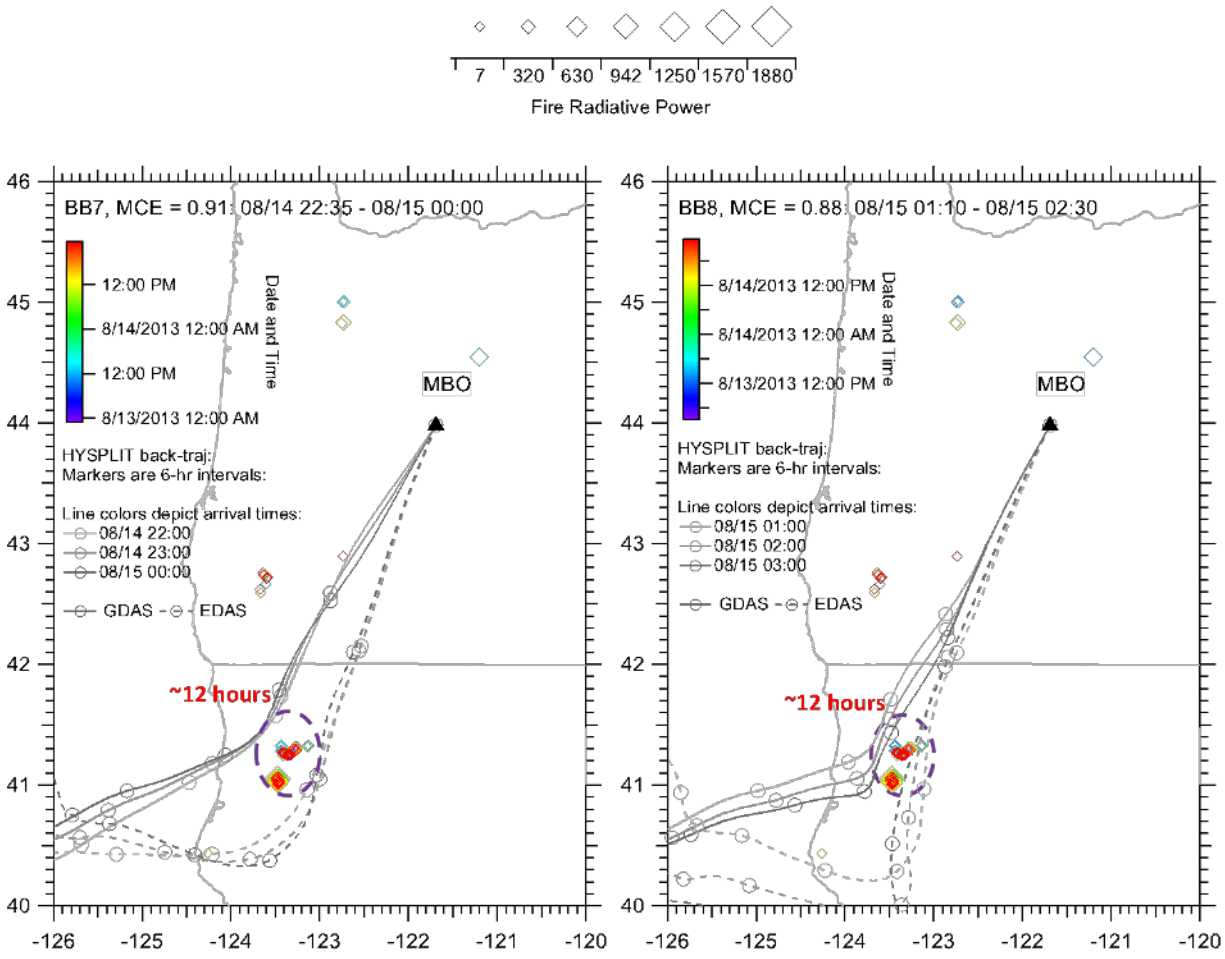

Figure S11: MBO Plumes BB7 and BB8 HYSPLIT 3-day back trajectory analysis using high-resolution meteorological field data (GDAS) and low-resolution meteorological field data (EDAS), markers are 6 hour intervals and trajectories are colored by arrival date and hour. MODIS fire dot data is superimposed and colored by time (PDT). MCE and plume interval are provided in the top left. Approximate plume transport times are estimated for likely plume candidates in red text.

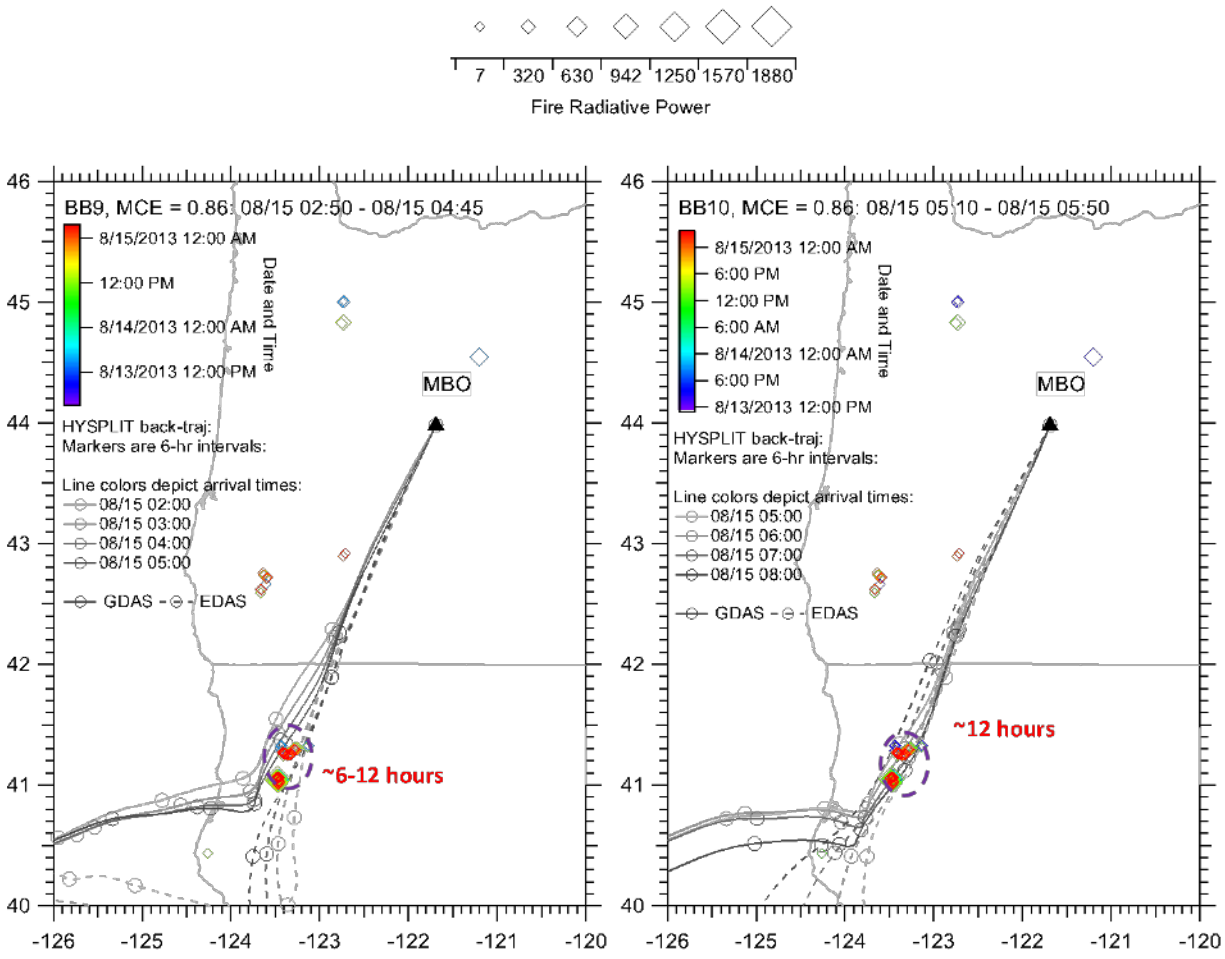

Figure S12: MBO Plumes BB9 and BB10 HYSPLIT 3-day back trajectory analysis using high-resolution meteorological field data (GDAS) and low-resolution meteorological field data (EDAS), markers are 6 hour intervals and trajectories are colored by arrival date and hour. MODIS fire dot data is superimposed and colored by time (PDT). MCE and plume interval are provided in the top left. Approximate plume transport times are estimated for likely plume candidates in red text.

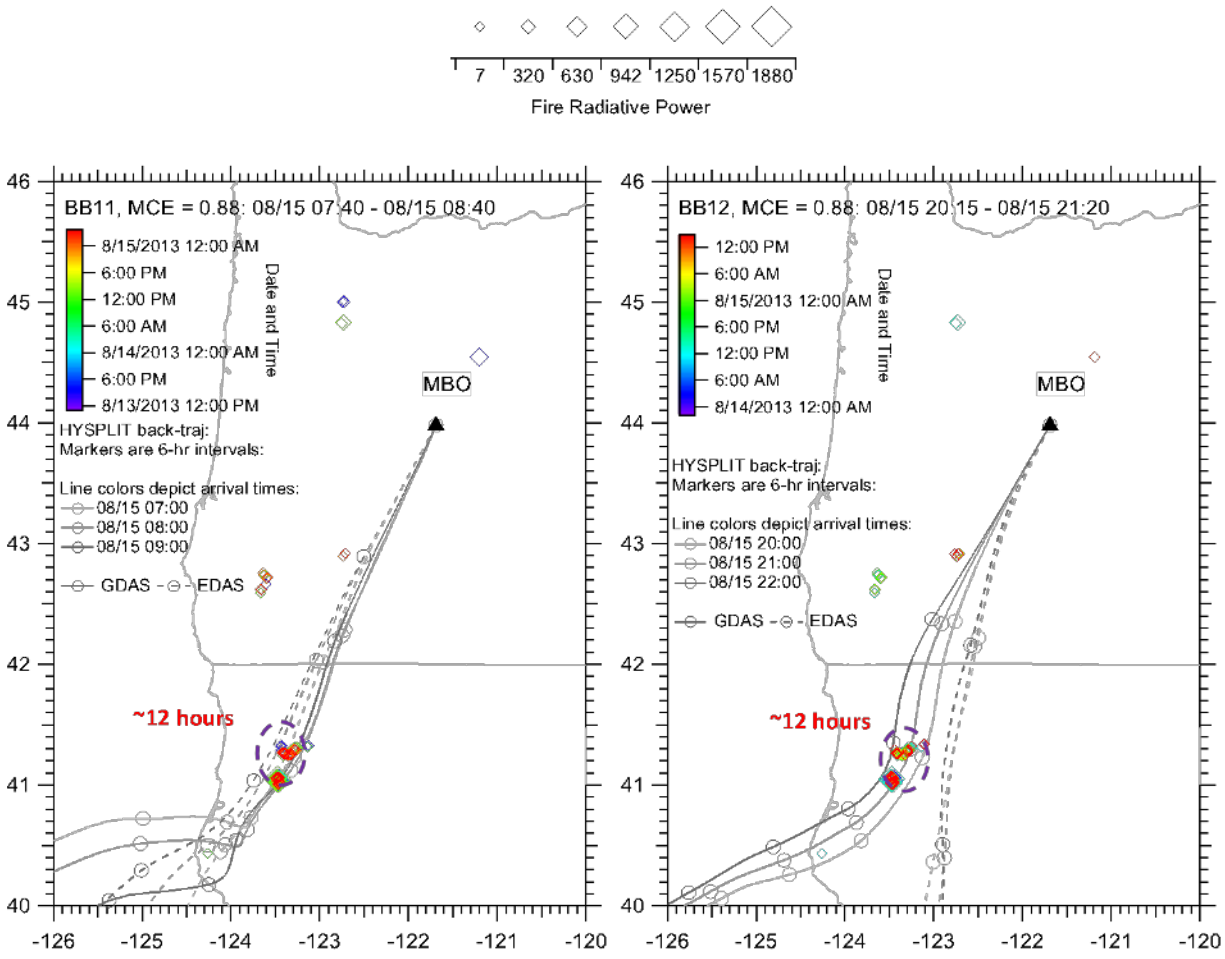

Figure S13: MBO Plumes BB11 and BB12 HYSPLIT 3-day back trajectory analysis using high-resolution meteorological field data (GDAS) and low-resolution meteorological field data (EDAS), markers are 6 hour intervals and trajectories are colored by arrival date and hour. MODIS fire dot data is superimposed and colored by time (PDT). MCE and plume interval are provided in the top left. Approximate plume transport times are estimated for likely plume candidates in red text.

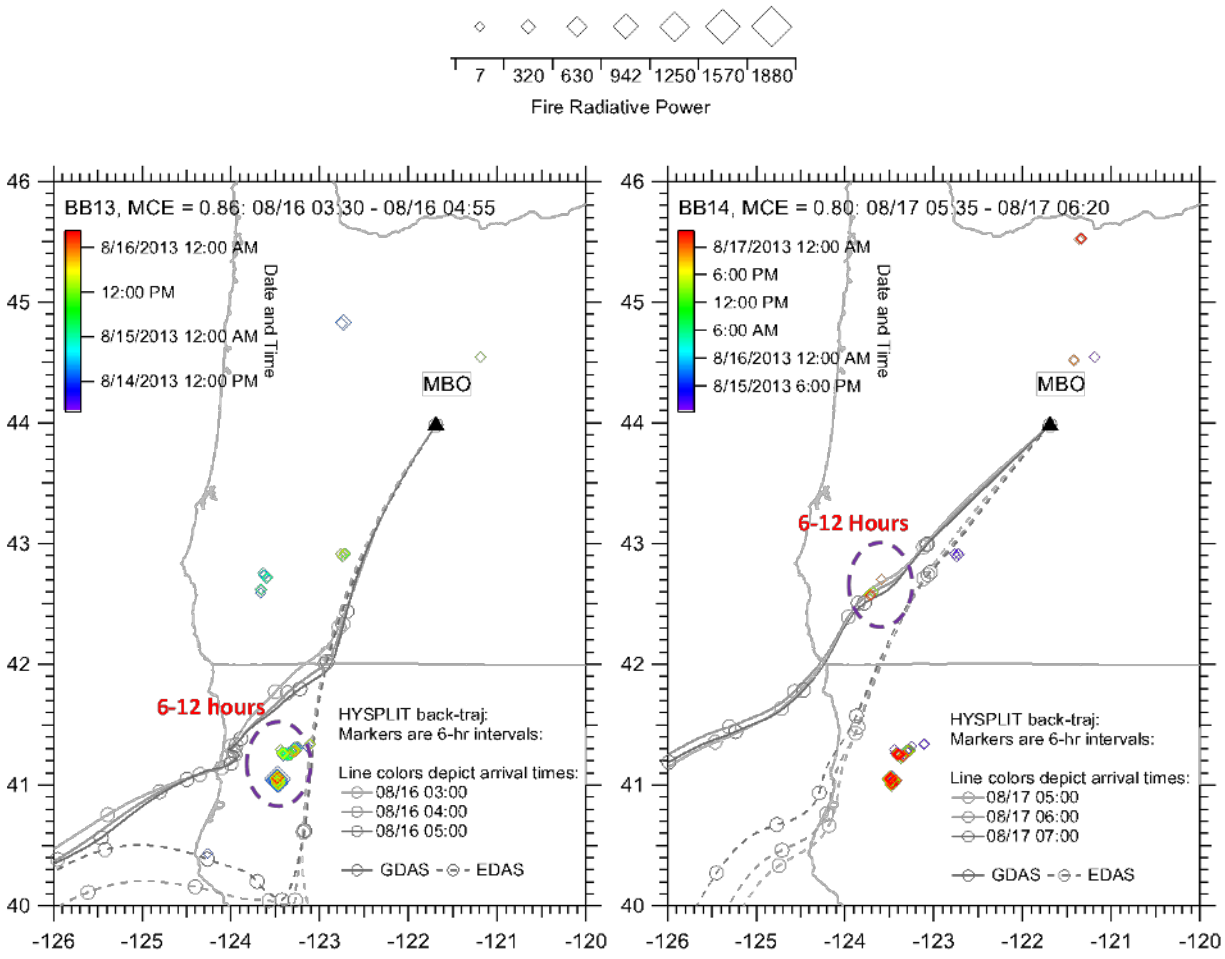

Figure S14: MBO Plumes BB13 and BB14 HYSPLIT 3-day back trajectory analysis using high-resolution meteorological field data (GDAS) and low-resolution meteorological field data (EDAS), markers are 6 hour intervals and trajectories are colored by arrival date and hour. MODIS fire dot data is superimposed and colored by time (PDT). MCE and plume interval are provided in the top left. Approximate plume transport times are estimated for likely plume candidates in red text.

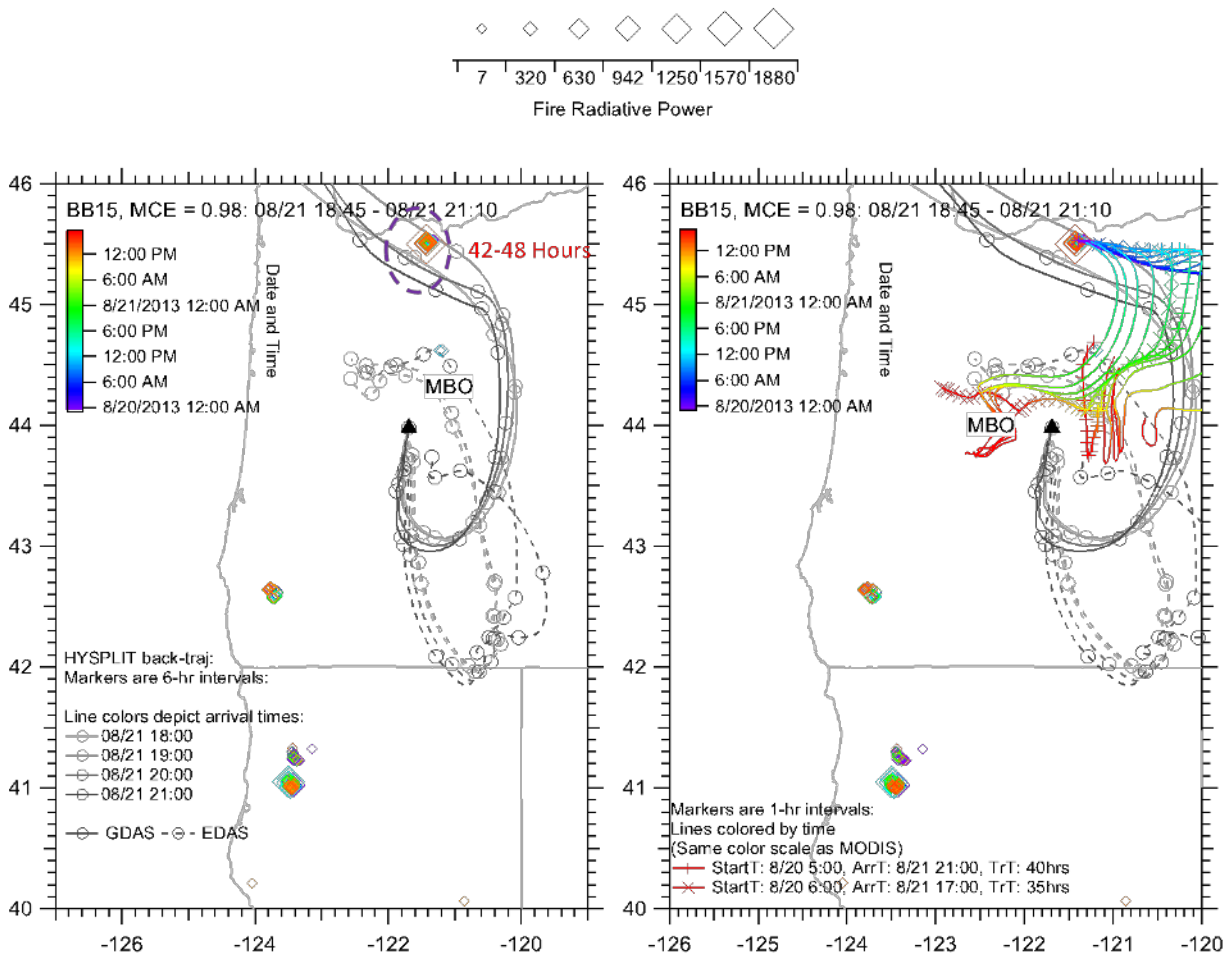

Figure S15: MBO Plume BB15 HYSPLIT 3-day back trajectory on the left and forward trajectory analysis on the right. Back trajectory uses high-resolution meteorological field data (GDAS) and low-resolution meteorological field data (EDAS), markers are 6 hour intervals and trajectories are colored by arrival date and hour (PDT). Estimated plume transport times are shown in red text and are based on back trajectory overlap with MODIS fire hotspot overlaps. Forward trajectory analyses (start times and locations based on back trajectory analysis results) use EDAS 40-km data and are colored by time (PDT) using same scale as MODIS fire hotspots. MODIS fire hotspot data is superimposed and colored by time (PDT). MCE and plume interval are provided in the top left. More refined plume transport times based on forward trajectory analyses shown in legend. Forward trajectories with markers denote trajectories where arrival time near MBO matches BB15 occurrence.

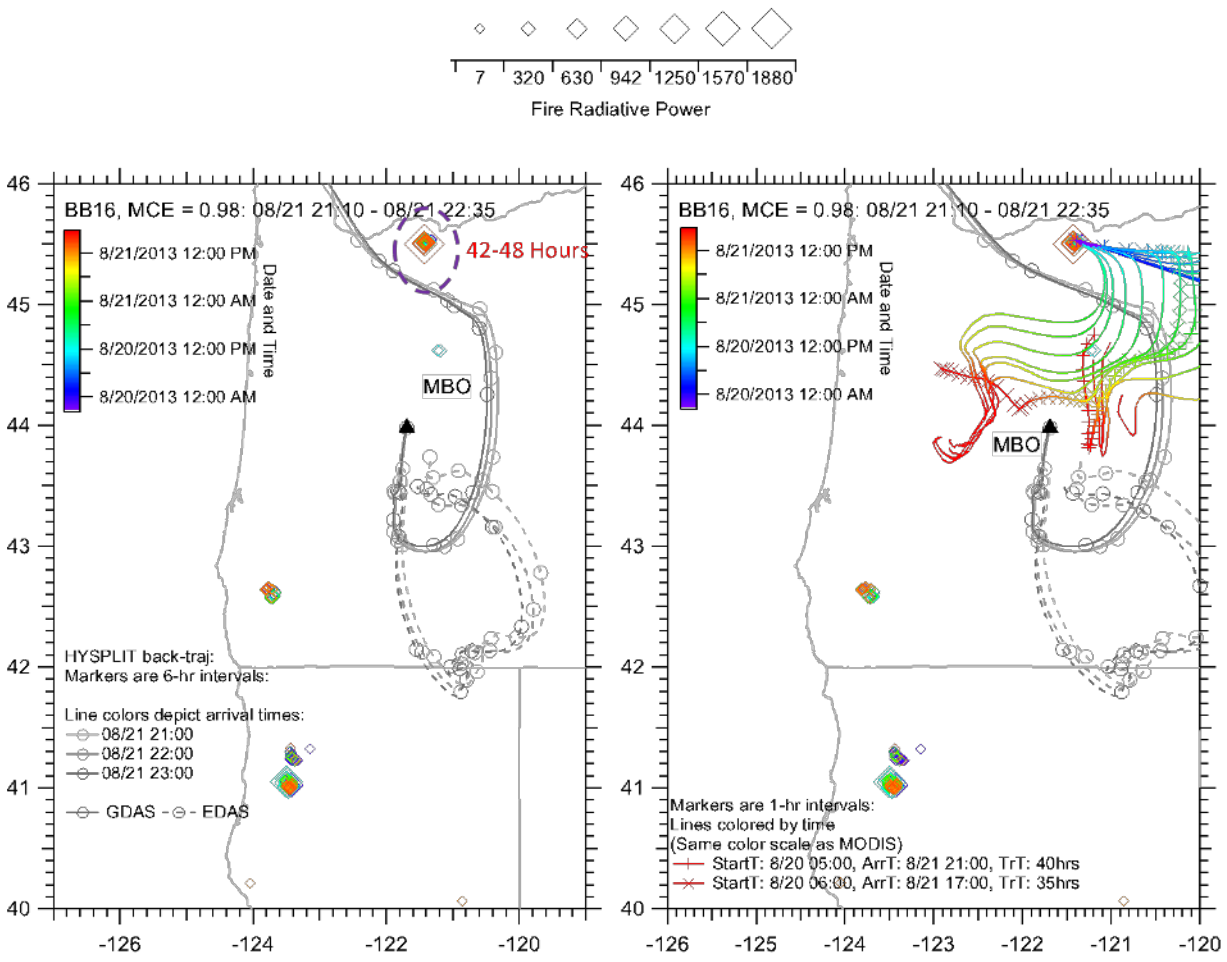

Figure S16: MBO Plume BB16 HYSPLIT 3-day back trajectory on the left and forward trajectory analysis on the right. Back trajectory uses high-resolution meteorological field data (GDAS) and low-resolution meteorological field data (EDAS), markers are 6 hour intervals and trajectories are colored by arrival date and hour (PDT). Estimated plume transport times are shown in red text and are based on back trajectory overlap with MODIS fire hotspot overlaps. Forward trajectory analyses (start times and locations based on back trajectory analysis results) use EDAS 40-km data and are colored by time (PDT) using same scale as MODIS fire hotspots. MODIS fire hotspot data is superimposed and colored by time (PDT). MCE and plume interval are provided in the top left. More refined plume transport times based on forward trajectory analyses shown in legend. Forward trajectories with markers denote trajectories where arrival time near MBO matches BB16 occurrence.

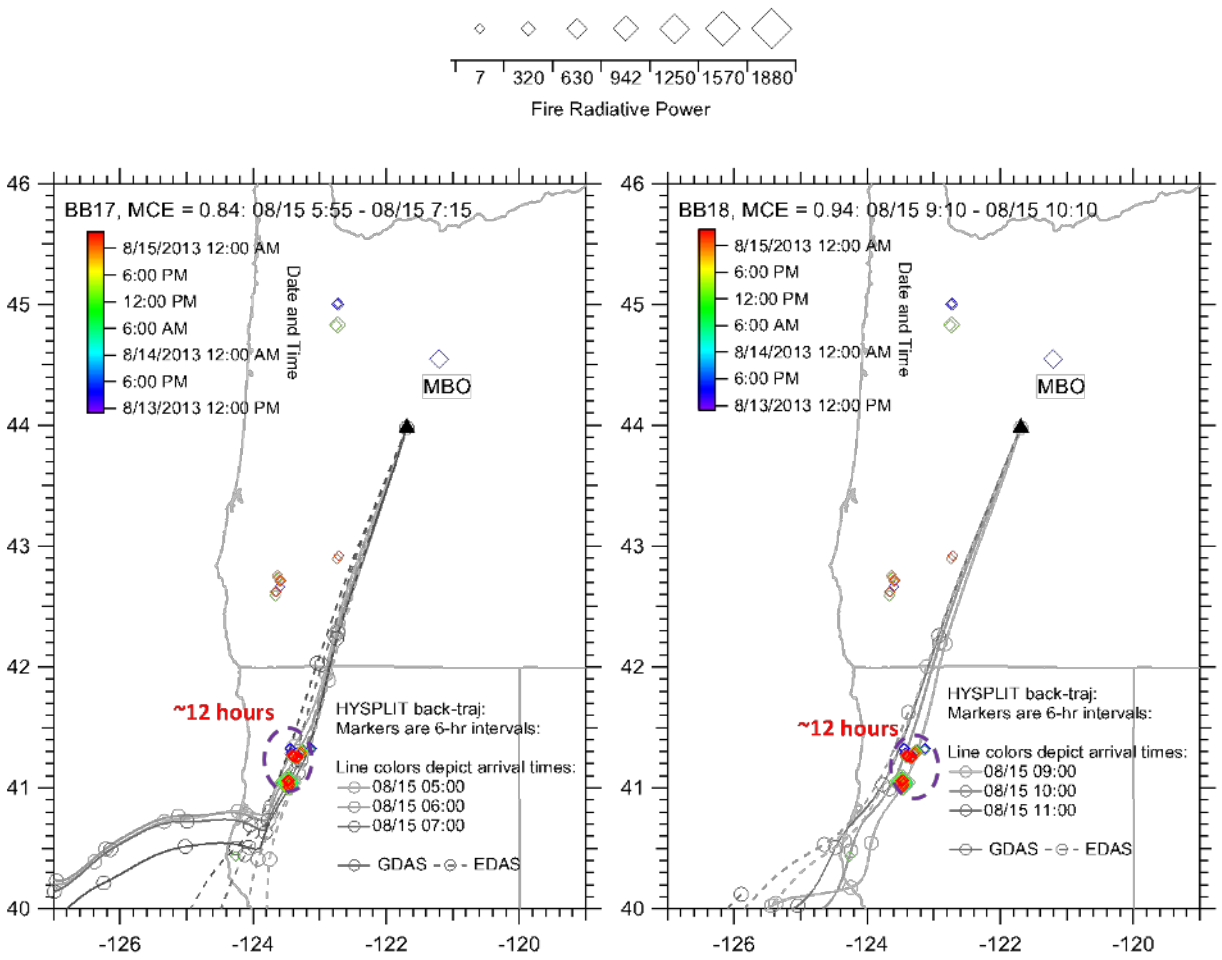

Figure S17: MBO Plumes BB17 and BB18 HYSPLIT 3-day back trajectory analysis using high-resolution meteorological field data (GDAS) and low-resolution meteorological field data (EDAS), markers are 6 hour intervals and trajectories are colored by arrival date and hour. MODIS fire dot data is superimposed and colored by time (PDT). MCE and plume interval are provided in the top left. Approximate plume transport times are estimated for likely plume candidates in red text.

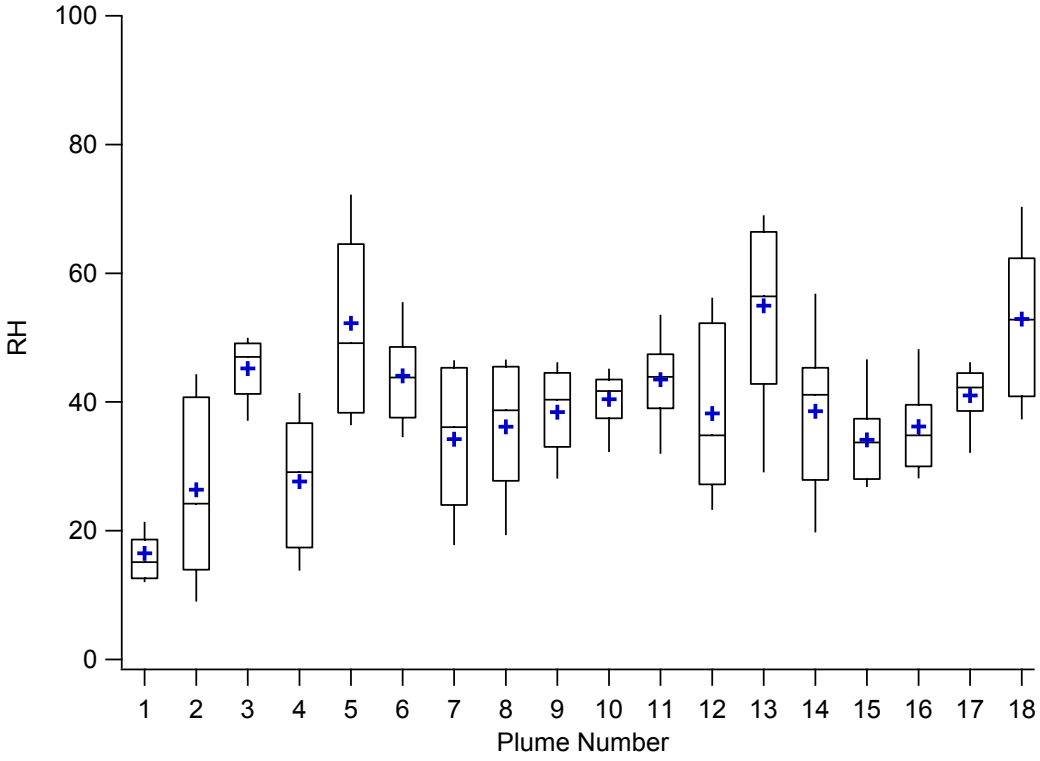

Figure S18: The box plots represent the statistical distribution of RH values extracted for back-trajectories from the HYSPLIT analysis of MCE candidate plumes arriving at MBO. The box and whiskers represent the 25th, 75th and 10th and 90th percentile values respectively. The blue crosses represent the mean and the black line within boxes represents the median values.

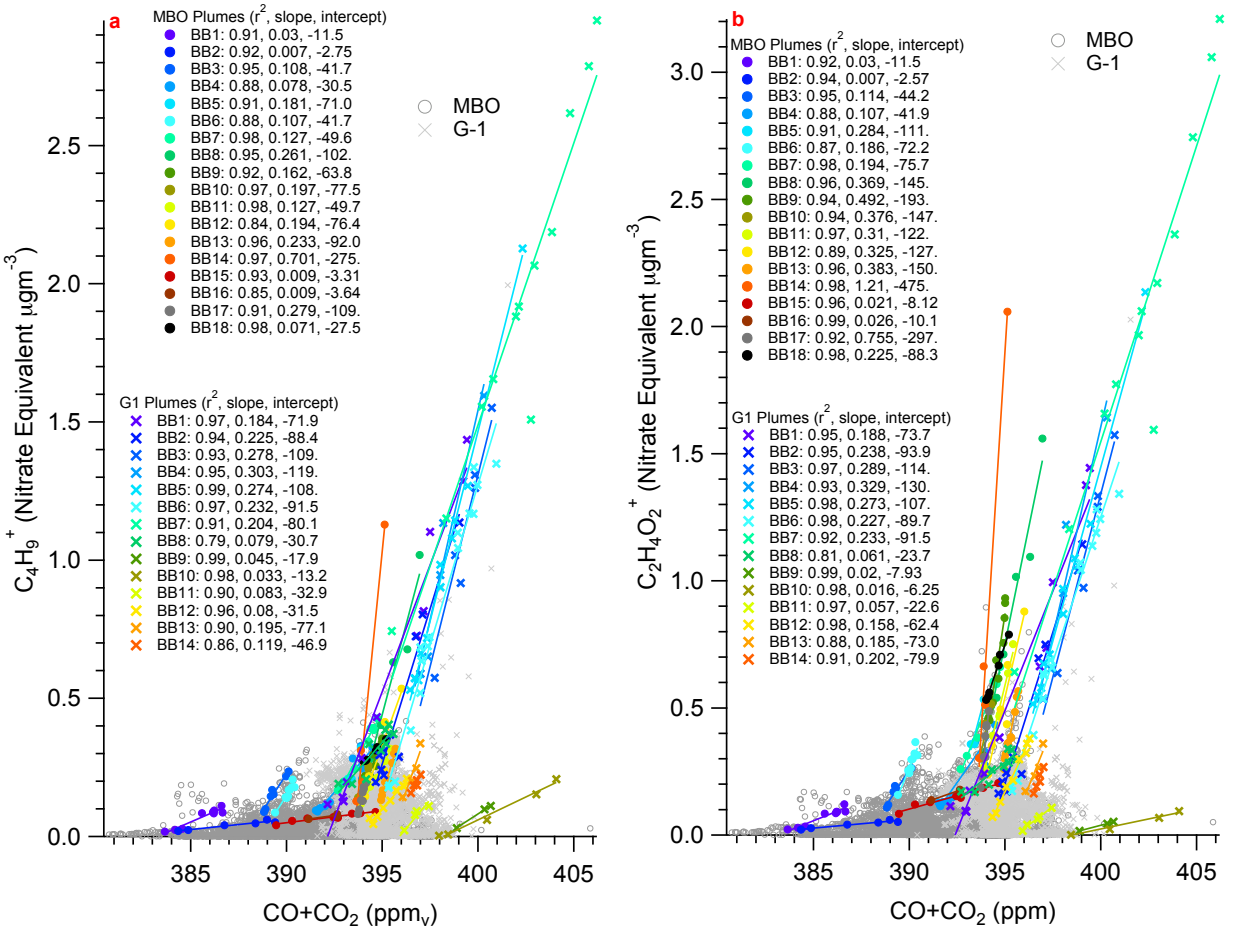

Figure S19: Scatter plots of (a) the ion tracer for hydrocarbons $C_4H_9^+$and (b) the ion tracer for levoglucosan, $C_2H_4O_2^+$ expressed as percent of total contribution to the high resolution organic mass spectrum, with respect to $CO+CO_2$. Units are in Nitrate equivalent $\mu gm^{-3}/ppm_v$. Enhancement ratios for individual plumes measured at MBO and by the G-1 aircraft are highlighted by colored markers and individual Pearson's r^2, slope and intercepts are provided in the legend.

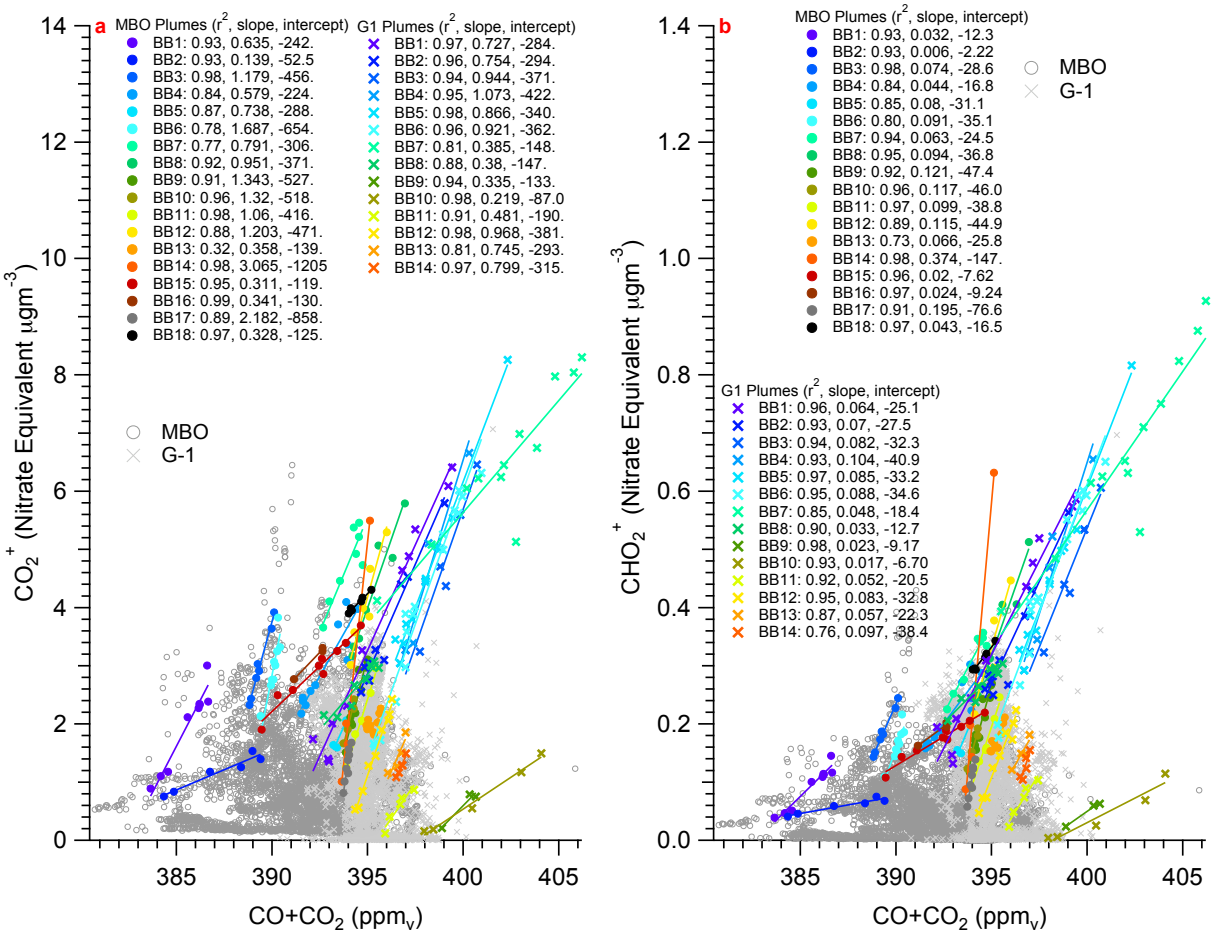

Figure S20: Scatter plots of the particulate matter (a) ion tracer for oxidation and organic acids, CO_2^+, and (b) ion tracer for organic acids CHO_2^+, both expressed as percent of total contribution to the high resolution organic mass spectrum, with respect to $CO+CO_2$. Units are in Nitrate equivalent $\mu gm^{-3}/ppm_v$. Enhancement ratios for individual plumes measured at MBO and by the G-1 aircraft are highlighted by colored markers and individual Pearson's r^2, slope and intercepts are provided in the legend.

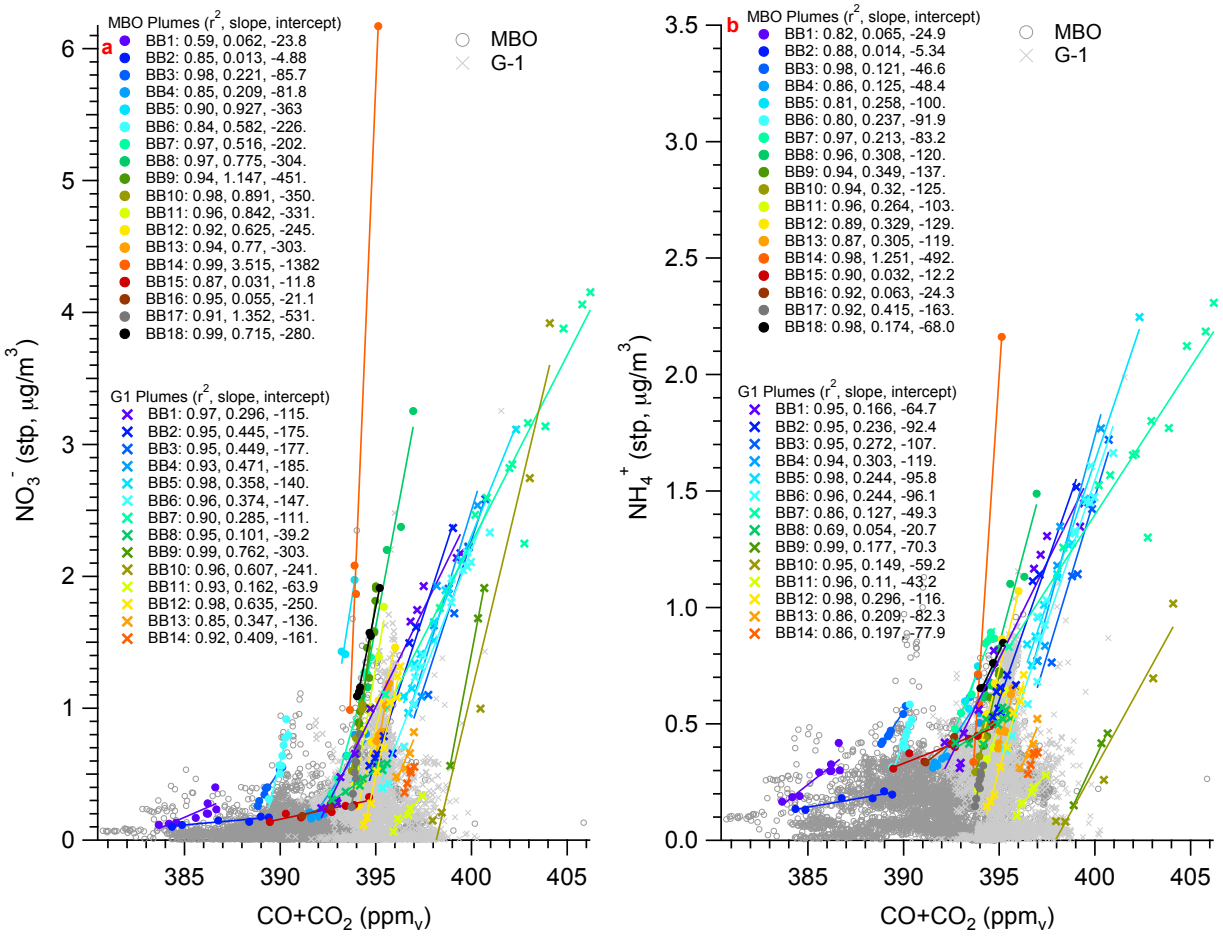

Figure S21: Scatter plots of particle phase inorganic (a) nitrate and (b) ammonium with respect to $CO+CO_2$. Units are in $\mu gm^{-3}/ppm_v$ and particulate component concentration has been converted to standard temperature and pressure. Enhancement ratios for individual plumes measured at MBO and by the G-1 aircraft are highlighted by colored markers and individual Pearson's r^2, slope and intercepts are provided in the legend.

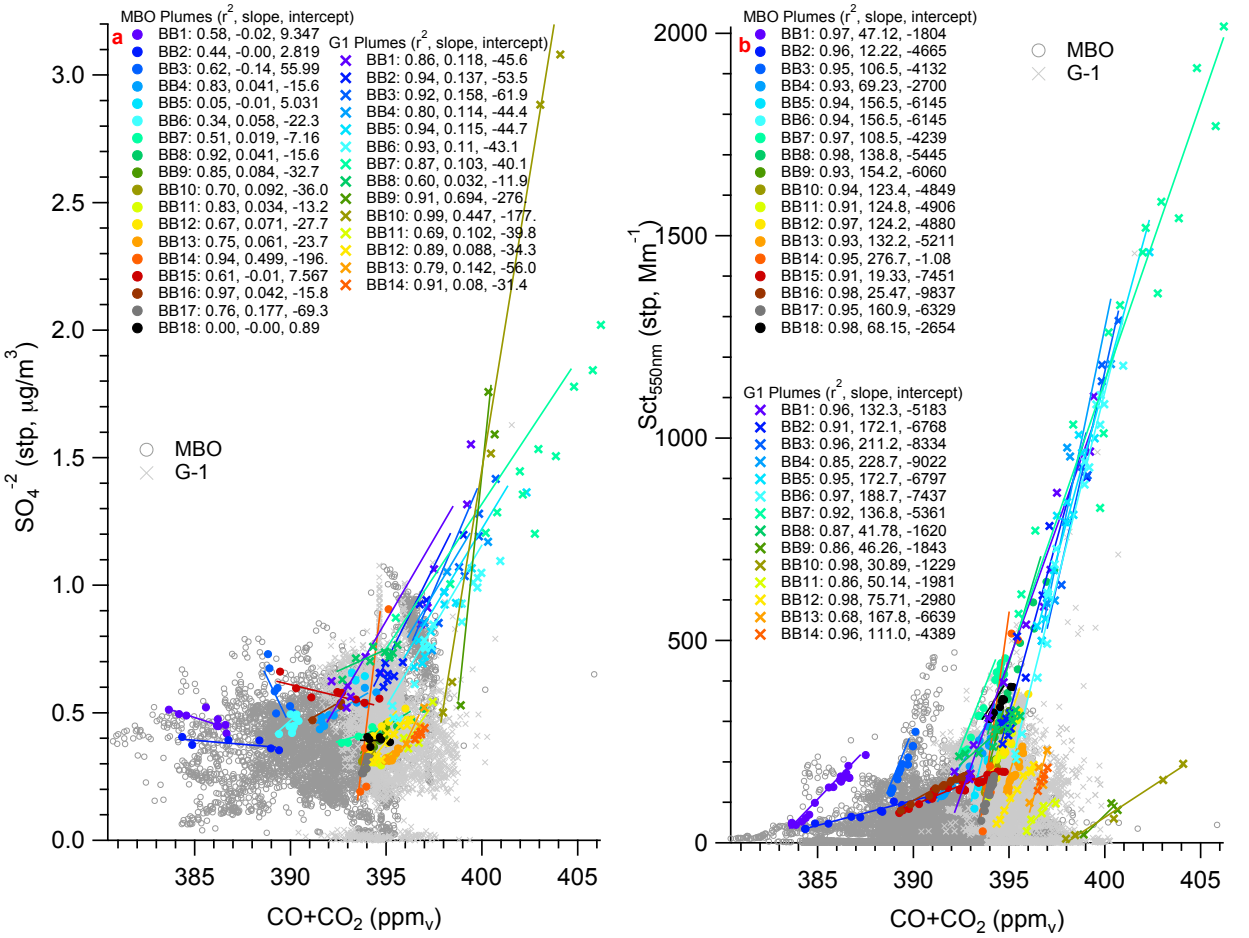

Figure S22: Scatter plots of (a) particle phase inorganic sulfate, and (b) optical scattering (550 nm wavelength), with respect to $CO+CO_2$. Units are in $\mu gm^{-3}/ppm_v$ and Mm^{-1}/ppm_v respectively. Enhancement ratios for individual plumes measured at MBO and by the G-1 aircraft are highlighted by colored markers and individual Pearson's r^2, slope and intercepts are provided in the legend.

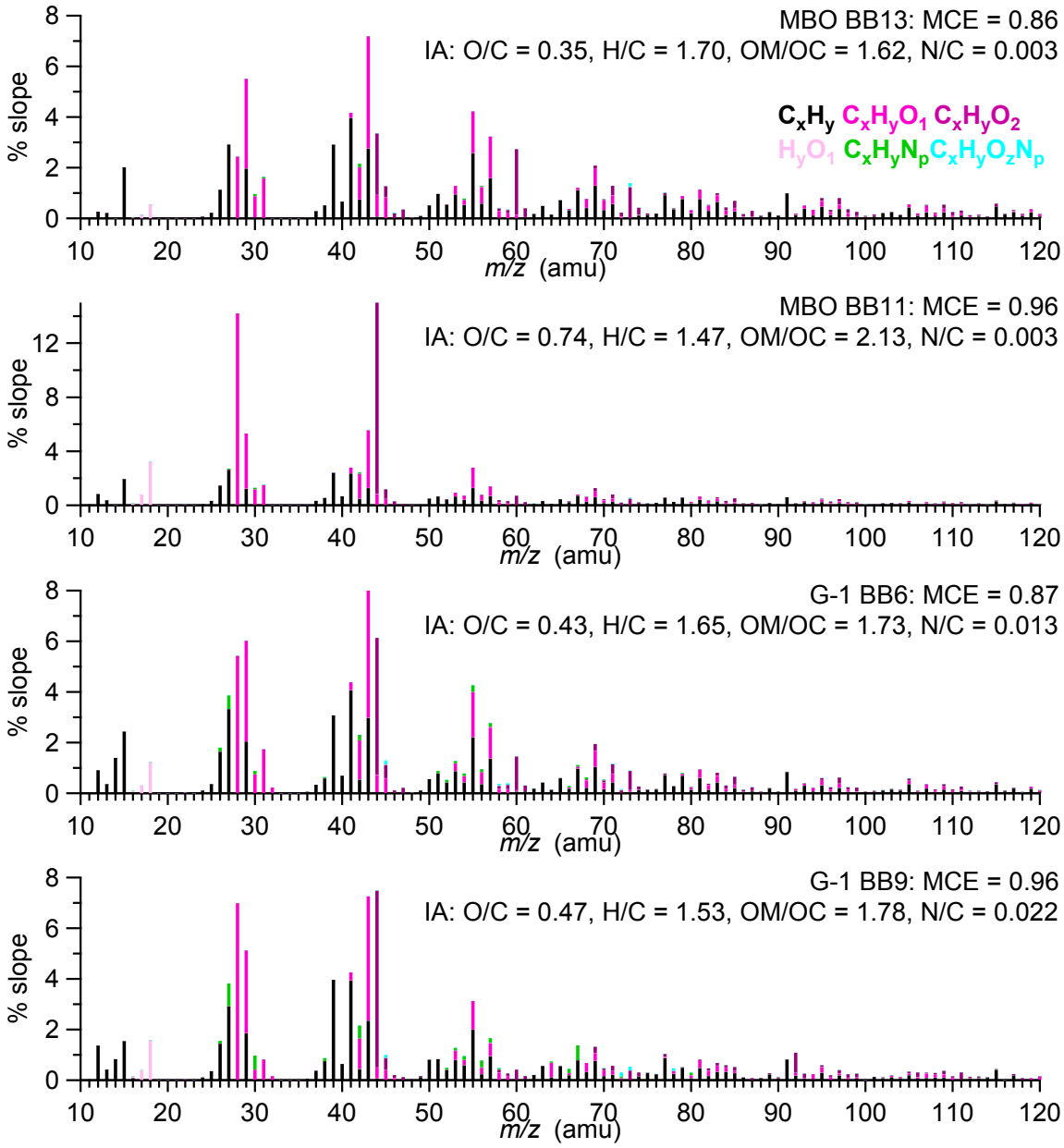

Figure S23: High resolution mass spectra of individual plumes from MBO (top two MS) and G-1 (bottom two MS). The mass spectral signals are displayed as unit mass resolution information with contributions from ion family classes separated by color and stacked at each m/z. The improved ambient method for calculation of elemental ratios [12] is used and reported in top right of MS.

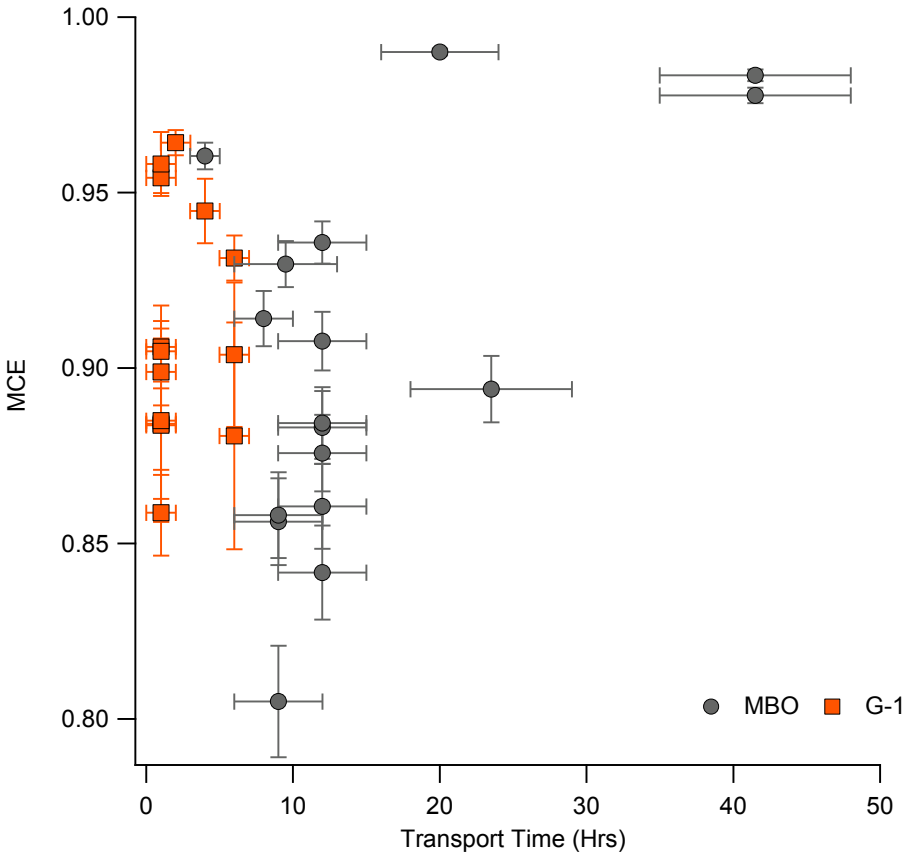

Figure S24: MCE values plotted as a function of transport time (hours). Error bars for MCE include measurement uncertainty as well as slope standard deviation (see caption for Table S2). Transport time ranges are based on HYSPLIT trajectory analysis (see Figures S3-S17). The information provided demonstrates that there is no discernible correlation between MCE and transport time.

4. Tables (S1 – S3)

Table S1: Summary of detection limit values derived from blank filter tests and calibration values derived for AMS from 3 calibration tests performed in the field and SP-AMS detection limits from 8 calibration tests performed in the field.

MBO High Resolution Aerosol MS	
Species	**Detection Limit (5 min averaging) μgm^{-3}**
Organics	0.16
SO_4^{-2}	0.0045
NO_3^-	0.0023
NH_4^+	0.0096
Chl^-	0.003
Calibration Type	**Calibration Value**
Ionization Efficiency	1.27E-07 (average of 3 IE tests)
IE/AB	6.64E-13
Average FlowRate (cc/s)	1.385
RIE NH_4	5
RIE SO_4	1.32
RIE NO_3	1.1

G-1 Soot Particle Aerosol MS†	
Species	**Detection Limit (1 second averaging) μgm^{-3}**
Organics	0.48
SO_4^{-2}	0.047
NO_3^-	0.05
NH_4^+	0.082
Chl^-	0.12
Calibration Type	**Calibration Value**
Ionization Efficiency	8.05E-08 (average of 8 IE tests)
IE/AB	6.27E-13
Average FlowRate (cc/s)	1.40+/- 0.01
RIE NH_4	3.3
RIE SO_4	1.2*
RIE NO_3	1.1

† Sampled from a pressure controlled inlet

*assumed typical fragmentation table value

Table S2: Summary of individual plume characteristics: plume ID, beginning and end date, duration in hours or seconds, MCE and MCE error, r^2 correlation, slope and slope error (1-σ) for CO vs CO_2, Organic PM_1 (STP) mass vs ΣC from Fig. 2a-2b in main text, and Organic PM_1 (STP) mass vs CO for both MBO (Top) and G-1 (bottom). MCE error is based on propagating the error of the slope standard deviation with the 1-sigma precision measurement for CO and CO_2 (1 ppb and 0.1 ppm respectively). First $\Delta CO/\Delta CO_2$ is calculated along with slope standard deviation (column 7) based on orthogonal linear regression. The propagated uncertainty of $\Delta CO/\Delta CO_2$ is $\sigma_{\Delta CO/\Delta CO2} = \Delta CO/\Delta CO_2 * [(\sigma_{slp})^2 + 0.1^2 + 0.001^2]^{1/2}$. The MCE = $1/(1+ \Delta CO/\Delta CO_2)$ and MCE error is calculated by taking the derivative of the equation for MCE where $\sigma_{MCE} = (1/(1+\Delta CO/\Delta CO_2)^2) * \sigma_{\Delta CO/\Delta CO2}$. Approximate transport time is provided for all plumes wherever a reasonable overlap of back and/or forward trajectory results and MODIS fire hotspots was observed. Wind direction is added for MBO in top portion of table. Note that plume numbers for MBO data are not related to plume numbers for G-1 data.

Plume ID	MBO Plume Period (PDT)		Dur (hrs)	MCE	CO vs CO_2 ppb/ppm		Org vs ΣC µgm^{-3}/ppm		Org vs CO µgm^{-3}/ppb		Est. Tr.T. (hrs)	WD
					r^2	Slope	r^2	Slope	r^2	Slope		
BB1	7/29/2013 18:35	7/29/2013 20:05	1.50	0.96±0.0038	0.97	41 ± 1.9	0.93	10 ± 1.1	0.98	0.24 ± 0.013	4 ± 1	W
BB2	7/30/2013 23:25	7/31/2013 0:25	1.00	0.99±0.0010	0.95	10 ± 0.70	0.93	2.1 ± 0.30	0.97	0.21 ± 0.018	20 ± 4	S/SW
BB3	8/5/2013 10:00	8/5/2013 11:05	1.08	0.91±0.0079	0.96	94 ± 5.7	0.97	25 ± 1.8	0.96	0.28 ± 0.026	8 ± 2	SW
BB4	8/7/2013 1:10	8/7/2013 3:00	1.83	0.93±0.0066	0.90	76 ± 5.5	0.86	18 ± 2.4	0.95	0.24 ± 0.018	10 ± 4	W
BB5	8/9/2013 8:00	8/9/2013 8:30	0.50	0.85±0.016	0.94	180 ± 23	0.90	44 ± 15	0.85	0.31 ± 0.12	Amb	E
BB6	8/14/2013 9:15	8/14/2013 10:50	1.58	0.89±0.0095	0.97	120 ± 5.4	0.84	36 ± 5.9	0.92	0.30 ± 0.034	24 ± 6	SW
BB7	8/14/2013 22:35	8/15/2013 0:00	1.42	0.91±0.0084	0.97	99 ± 4.1	0.98	25 ± 1.4	0.99	0.27 ± 0.0076	12 ± 3	SW
BB8	8/15/2013 1:20	8/15/2013 2:30	1.17	0.88±0.011	0.98	140 ± 5.2	0.96	44 ± 4.0	0.98	0.34 ± 0.022	12 ± 3	SW
BB9	8/15/2013 2:50	8/15/2013 4:45	1.92	0.86±0.012	0.95	170 ± 8.7	0.95	50 ± 3.7	0.98	0.33 ± 0.014	9 ± 3	SW
BB10	8/15/2013 5:10	8/15/2013 5:50	0.67	0.86±0.012	0.97	160 ± 12	0.98	44 ± 4.6	1.00	0.31 ± 0.0092	12 ± 3	SW
BB11	8/15/2013 7:40	8/15/2013 8:40	1.00	0.88±0.010	0.95	130 ± 9.9	0.99	34 ± 2.0	0.94	0.28 ± 0.037	12 ± 3	SW
BB12	8/15/2013 20:15	8/15/2013 21:20	1.08	0.88±0.010	0.98	130 ± 5.3	0.85	46 ± 9.4	0.89	0.36 ± 0.062	12 ± 3	SW
BB13	8/16/2013 3:30	8/16/2013 4:55	1.42	0.86±0.012	0.96	170 ± 8.8	0.92	36 ± 4.0	0.98	0.24 ± 0.012	9 ± 3	SW
BB14	8/17/2013 5:35	8/17/2013 6:20	0.75	0.80±0.016	0.97	240 ± 16	0.98	130 ± 13	1.00	0.63 ± 0.020	9 ± 3	SW
BB15	8/21/2013 18:45	8/21/2013 21:10	2.42	0.98±0.0016	0.92	17 ± 1.0	0.96	4.7 ± 0.40	0.95	0.29 ± 0.024	42 ± 7	SW
BB16	8/21/2013 21:10	8/21/2013 22:35	1.42	0.98±0.0022	0.99	23 ± 0.60	1.00	4.9 ± 0.033	1.00	0.25 ± 0.014	42 ± 7	SW
BB17	8/15/2013 5:55	8/15/2013 7:15	1.33	0.84±0.013	0.97	190 ± 8.3	0.92	80 ± 9.5	0.94	0.47 ± 0.049	12 ± 3	SW
BB18	8/15/2013 9:10	8/15/2013 10:10	1.00	0.94±0.0060	0.98	69 ± 2.9	0.99	18 ± 0.81	0.98	0.27 ± 0.019	12 ± 3	SW

Plume ID	G1 Plume Period (PDT)		Dur (sec)	MCE	CO vs CO_2 ppb/ppm		Org vs ΣC µgm^{-3}/ppm		Org vs CO µgm^{-3}/ppb		Est. Tr.T. (hrs)
					r^2	Slope	r^2	Slope	r^2	Slope	
BB1	8/6/2013 13:05	8/6/2013 13:06	60	0.90±0.0095	0.90	110 ± 12	0.98	26 ± 1.2	0.98	0.26 ± 0.019	1 ± 1
BB2	8/6/2013 13:19	8/6/2013 13:20	60	0.91±0.012	0.84	104 ± 14	0.96	31 ± 2.3	0.96	0.31 ± 0.065	1 ± 1
BB3	8/6/2013 13:34	8/6/2013 13:34	35	0.88±0.015	0.91	130 ± 19	0.96	39 ± 3.6	0.96	0.33 ± 0.050	1 ± 1
BB4	8/6/2013 13:34	8/6/2013 13:35	35	0.88±0.028	0.74	130 ± 35	0.96	44 ± 4.7	0.96	0.39 ± 0.10	1 ± 1
BB5	8/6/2013 13:35	8/6/2013 13:36	65	0.89±0.022	0.65	130 ± 29	0.99	36 ± 1.0	0.99	0.32 ± 0.067	1 ± 1
BB6	8/6/2013 13:36	8/6/2013 13:37	85	0.86±0.012	0.92	160 ± 12	0.98	34 ± 1.3	0.98	0.24 ± 0.013	1 ± 1
BB7	8/6/2013 13:45	8/6/2013 13:46	80	0.90±0.0086	0.93	110 ± 7.8	0.90	26 ± 2.7	0.90	0.24 ± 0.040	1 ± 1
BB8	8/6/2013 13:56	8/6/2013 13:57	50	0.95±0.0044	0.96	48 ± 3.6	0.88	14 ± 2.0	0.88	0.27 ± 0.027	1 ± 1
BB9	8/6/2013 14:58	8/6/2013 14:58	15	0.96±0.0091	0.95	44 ± 9.9	0.98	8.7 ±1.3	0.98	0.21 ± 0.013	1 ± 1
BB10	8/6/2013 14:58	8/6/2013 14:58	25	0.96±0.0036	0.97	37 ± 3.8	0.96	6.5 ± 0.76	0.96	0.17 ± 0.037	2 ± 1
BB11	8/16/2013 12:24	8/16/2013 12:25	25	0.94±0.0092	0.91	59 ± 10	0.92	16 ± 2.7	0.92	0.29 ± 0.018	4 ± 1
BB12	8/16/2013 12:49	8/16/2013 12:50	45	0.93±0.0064	0.99	74 ± 2.7	0.99	26 ± 1.0	0.99	0.37 ± 0.020	6 ± 1
BB13	8/16/2013 12:51	8/16/2013 12:52	20	0.90±0.021	0.90	110 ± 25	0.86	33 ± 9.4	0.86	0.29 ± 0.13	6 ± 1
BB14	8/16/2013 12:52	8/16/2013 12:52	25	0.88±0.032	0.78	140 ± 42	0.97	29 ± 3.1	0.97	0.25 ± 0.059	6 ± 1

Table S3: Summary of emission factor values provided by previous studies and reviews using similar biomes and/or fuels and plotted in Figure 6 of the main text. The emission ratio of OC to total carbon as ΣC is calculated as: $^{\Delta OC}/_{\Delta \sum C} = \frac{\Delta OC}{\Delta CO_2 \times (^{12}/_{44}) + \Delta CO \times (^{12}/_{28})}$

The error is calculated by adding in quadrature.

						Emission Ratio ΔOC/ΔΣC, gC/gC	Error
Akagi et al. 2011	**MCE**	Not provided					
Review	**OC**	9.2	±	0.78	g/kg dry fuel burned	0.020	0.0074
Extratropical Forest	**CO**	122	±	44	g/kg dry fuel burned		
	CO_2	1509	±	98	g/kg dry fuel burned		
McMeeking et al. 2009	**MCE**	0.92	±	0.068			
Lab study	**OC**	7.8	±	7.2	g/kg dry fuel burned	0.020	0.022
Boreal Forest	**CO**	71	±	40	g/kg dry fuel burned		
	CO_2	1311	±	325	g/kg dry fuel burned		
Alves et al. 2011	**MCE**	0.87	±	0.1			
Field	**OC**	6	±	2.9	g/kg dry fuel burned	0.013	0.0087
Mixed-Evergreen Forest	**CO**	170	±	83	g/kg dry fuel burned		
	CO_2	1485	±	147	g/kg dry fuel burned		

5. References

1. Wigder, N. L.; Jaffe, D. A.; Saketa, F. A., Ozone and particulate matter enhancements from regional wildfires observed at Mount Bachelor during 2004–2011. *Atmospheric Environment* **2013,** *75*, (0), 24-31.
2. Weiss-Penzias, P.; Jaffe, D. A.; Swartzendruber, P.; Dennison, J. B.; Chand, D.; Hafner, W.; Prestbo, E., Observations of Asian air pollution in the free troposphere at Mount Bachelor Observatory during the spring of 2004. *Journal of Geophysical Research: Atmospheres* **2006,** *111*, (D10), D10304.
3. Ambrose, J. L.; Reidmiller, D. R.; Jaffe, D. A., Causes of high O3 in the lower free troposphere over the Pacific Northwest as observed at the Mt. Bachelor Observatory. *Atmospheric Environment* **2011,** *45*, (30), 5302-5315.
4. Liu, Y., Variability of wildland fire emissions across the contiguous United States. *Atmospheric Environment* **2004,** *38*, (21), 3489-3499.
5. Fischer, E. V.; Jaffe, D. A.; Reidmiller, D. R.; Jaeglé, L., Meteorological controls on observed peroxyacetyl nitrate at Mount Bachelor during the spring of 2008. *Journal of Geophysical Research: Atmospheres* **2010,** *115*, (D3), D03302.
6. Fischer, E. V.; Hsu, N. C.; Jaffe, D. A.; Jeong, M. J.; Gong, S. L., A decade of dust: Asian dust and springtime aerosol load in the U.S. Pacific Northwest. *Geophysical Research Letters* **2009,** *36*, (3), n/a-n/a.
7. DeCarlo, P. F.; Kimmel, J. R.; Trimborn, A.; Northway, M. J.; Jayne, J. T.; Aiken, A. C.; Gonin, M.; Fuhrer, K.; Horvath, T.; Docherty, K. S.; Worsnop, D. R.; Jimenez, J. L., Field-Deployable, High-Resolution, Time-of-Flight Aerosol Mass Spectrometer. *Analytical Chemistry* **2006,** *78*, (24), 8281-8289.
8. Jimenez, J. L.; Canagaratna, M. R.; Donahue, N. M.; Prevot, A. S. H.; Zhang, Q.; Kroll, J. H.; DeCarlo, P. F.; Allan, J. D.; Coe, H.; Ng, N. L.; Aiken, A. C.; Docherty, K. S.; Ulbrich, I. M.; Grieshop, A. P.; Robinson, A. L.; Duplissy, J.; Smith, J. D.; Wilson, K. R.; Lanz, V. A.; Hueglin, C.; Sun, Y. L.; Tian, J.; Laaksonen, A.; Raatikainen, T.; Rautiainen, J.; Vaattovaara, P.; Ehn, M.; Kulmala, M.; Tomlinson, J. M.; Collins, D. R.; Cubison, M. J.; E.; Dunlea, J.; Huffman, J. A.; Onasch, T. B.; Alfarra, M. R.; Williams, P. I.; Bower, K.; Kondo, Y.; Schneider, J.; Drewnick, F.; Borrmann, S.; Weimer, S.; Demerjian, K.; Salcedo, D.; Cottrell, L.; Griffin, R.; Takami, A.; Miyoshi, T.; Hatakeyama, S.; Shimono, A.; Sun, J. Y.; Zhang, Y. M.; Dzepina, K.; Kimmel, J. R.; Sueper, D.; Jayne, J. T.; Herndon, S. C.; Trimborn, A. M.; Williams, L. R.; Wood, E. C.; Middlebrook, A. M.; Kolb, C. E.; Baltensperger, U.; Worsnop, D. R., Evolution of Organic Aerosols in the Atmosphere. *Science* **2009,** *326*, (5959), 1525-1529.
9. Grieshop, A. P.; Donahue, N. M.; Robinson, A. L., Laboratory investigation of photochemical oxidation of organic aerosol from wood fires 2: analysis of aerosol mass spectrometer data. *Atmos. Chem. Phys.* **2009,** *9*, (6), 2227-2240.
10. Ortega, A. M.; Day, D. A.; Cubison, M. J.; Brune, W. H.; Bon, D.; de Gouw, J. A.; Jimenez, J. L., Secondary organic aerosol formation and primary organic aerosol oxidation from biomass-burning smoke in a flow reactor during FLAME-3. *Atmos. Chem. Phys.* **2013,** *13*, (22), 11551-11571.
11. Middlebrook, A. M.; Bahreini, R.; Jimenez, J. L.; Canagaratna, M. R., Evaluation of Composition-Dependent Collection Efficiencies for the Aerodyne Aerosol Mass Spectrometer using Field Data. *Aerosol Science and Technology* **2012,** *46*, 258–271.

12. Canagaratna, M. R.; Jimenez, J. L.; Kroll, J. H.; Chen, Q.; Kessler, S. H.; Massoli, P.; Hildebrandt Ruiz, L.; Fortner, E.; Williams, L. R.; Wilson, K. R.; Surratt, J. D.; Donahue, N. M.; Jayne, J. T.; Worsnop, D. R., Elemental ratio measurements of organic compounds using aerosol mass spectrometry: characterization, improved calibration, and implications. *Atmos. Chem. Phys.* **2015,** *15*, (1), 253-272.
13. Hand, J. L.; Malm, W. C., Review of aerosol mass scattering efficiencies from ground-based measurements since 1990. *Journal of Geophysical Research: Atmospheres* **2007,** *112*, (D16), D16203.
14. Aiken, A. C.; DeCarlo, P. F.; Jimenez, J. L., Elemental analysis of organic species with electron ionization high-resolution mass spectrometry. *Analytical Chemistry* **2007**.
15. Fischer, E.; Jaffe, D.; Marley, N.; Gaffney, J.; Marchany-Rivera, A., Optical properties of aged Asian aerosols observed over the US Pacific Northwest. *Journal of Geophysical Research: Atmospheres (1984–2012)* **2010,** *115*, (D20).
16. Briggs, N. L.; Jaffe, D. A.; Gao, H.; Hee, J.; Baylon, P.; Zhang, Q.; Zhou, S.; Collier, S.; Sampson, P.; Cary, R. A., Particulate matter, ozone, and nitrogen species in aged wildfire plumes observed at the Mount Bachelor Observatory, a high elevation site in the Pacific Northwest. *Aerosol and Air Quality Research* **2016,** *Accepted*.
17. McClure, C. D.; Jaffe, D. A.; Gao, H., Carbon Dioxide in the Free Troposphere and Boundary Layer at the Mt. Bachelor Observatory. *Aerosol and Air Quality Research* **2015**.
18. Anderson, T. L.; Ogren, J. A., Determining Aerosol Radiative Properties Using the TSI 3563 Integrating Nephelometer. *Aerosol Science and Technology* **1998,** *29*, (1), 57-69.